Cellulose Templated $Zn_{1-X}Cu_XO/Ag_2O$ Composite Photocatalyst for the Degradation of Methylene blue under Visible light irradiation

Biruktait Ayele Lemechu

Thesis Submitted to the department of Materials Science and Engineering
School of Mechanical, Chemical and Material Engineering

Presented in Partial Fulfillment of the Requirement for the Degree of Masters in Materials Science and Engineering

Office of Postgraduate Studies

Adama Science and Technology University

Adama, Ethiopia
July, 2020 G.C

Cellulose Templated $Zn_{1-X}Cu_XO/Ag_2O$ Composite Photocatalyst for the Degradation of Methylene blue under Visible Light irradiation

Biruktait Ayele Lemechu

Advisor

Osman Ahmed Zelekew (PhD)

Co-Advisor

Dinsefa Mensur Andoshe (PhD)

Department of Materials Science and Engineering

School of Mechanical, Chemical and Material Engineering

Presented in Partial Fulfillment of the Requirement for The Degree of Masters in Materials Science and Engineering

Office of Postgraduate Studies

Adama Science and Technology University

Adama

July, 2020 G.

Advisors Approval Sheet

To: Materials Science and Engineering Department

Subject: Thesis Submission

This is to certify that the thesis entitled on "Cellulose Templated $Zn_{1-X}Cu_XO/Ag_2O$ Composite Photocatalyst for the Degradation of Methylene blue under visible light irradiation" which is submitted in partial fulfillment of the requirements for the degree of Masters in Materials Science and Engineering, the post graduate program of the department of Materials Science and Engineering, and has been carried out by Miss Biruktait Ayele, Id. No pgr/18248/11, under our supervision. Therefore, we recommended that the student has fulfilled the requirements and hence hereby she can submit the thesis to the department.

…….	……	……..
Advisor	Signature	Date
……	……	……..
Co-advisor	Signature	Date

Declaration

Hereby, I declare that this M.Sc thesis is my original work and has not been presented for any degree in any other university, and all the source of materials used for this thesis have been duly acknowledged.

…….	..…….	…….
Student	signature	Date

Approval of Board of Examiners

We, the undersigned members of the board of examiners of the final open defense by Biruktait Ayele have read and evaluated her thesis entitled on "Cellulose Templated $Zn_{1-x}Cu_xO/Ag_2O$ Composite Photocatalyst for the Degradation of Methylene blue under visible light irradiation" and examined the candidate. Therefore, this is to certify that the thesis has been accepted in partial fulfillment of the degree of Masters.

…….	…….	……. …
Advisor	Signature	Date
……	…….	…….
Chairperson	Signature	Date
……	……	……..
Internal Examiner	Signature	Date
……	……	……
External Examiner	Signature	Date

ACKNOWLEDGMENT

First of all, I would like to thank GOD for his almightiness trough out my journey. Then after, I would like express my deep sense of gradtitude and respect to Dr. Osman Ahmed Zelekew, Dr. Dinsefa Mensur Andoshe and Dr Temesgen Debelo for their Bold, consistence, and, inspiring guidance, constructive criticism and valuable suggestions throughout this research work.

I am deeply indebted to my families, who always believed in me and gave all their support for all of choices that I have ever made. And my special thanks goes for Mr. Demeke Tesfaye, for his amazing patience, inspiring support and facilitation, throughout all of the lab activities of this research work. I would also like to extend my deep gratitude to all of my staff members, specially, Mr. Andualem Merga and Mr. Henok Girma, for their constructive advice, encouragement and true friendship supports throughout this research work. Lastly, but not least, I would like to thank Materials Science and Engineering Department and Adama Science and Technology university for providing this Masters scholarship.

Abstract

The wastewater textile, pulp, paper, and dyeing industries contains different kinds of organic dyes. These dyes have an enormous negative impact on human health and the whole ecosystem. Photocatalysis is the preferable way to degrade them. Accordingly, in this work, the $Zn_{1-x}Cu_xO/Ag_2O$ composite photocatalyst (CZA) were synthesized using biological renewable cellulose extracted from unwanted water hyacinth (Eichhornia crassipes) plant as a template and characterized by using different instruments. Two optimizations were performed to obtain the best catalyst. The first optimization resulted 2% Cu-ZnO catalyst (CZ-2) to have best photocatalytic performance (82%) over the photocatalytic activity of Z (33.38%), CZ-1 (63.25%), CZ-3 (64.59%) and CZ-4 (60.52%) on the degradation of methylene blue under visible light irradiation within 100 min. On the other hand, the highest photocatalytic activity was obtained from CZA-10.2 catalyst (92.48%) prepared from CZ-2 and Ag_2O with molar ratio of 10:1 after dried at 60 ^{0}C to form CZA composite catalyst within 24 hr. However, CZA-6.8, CZA-13.6, and CZA-20.4 composite catalysts could degrade 90.47%, 79.24%, and 79.0% of the dye respectively, within 100 min under visible light irradiation. Furthermore, the CZA-10.2 catalyst was confirmed to be stable through three consecutive rounds during reusability tests. Generally, The cellulose aided synthesis led to the formation of herarical CZA-10.2 catalyst, which enhances its adsorption capacity. However, Cu-doping was the key factor for the visible light responsive of ZnO and loading of Ag_2O on the surface of Cu-ZnO was further decreased the e^-/h^+ recombination. Hence, both doping of n-type ZnO with Cu and the formation of p-n hetrojunction with p-type Ag_2O simultaneously was enhanced the degradation of methylene blue under visible light irradiation. Furthermore, the effect of calcinations temperature on the photocatalytic performance of CZA-10.2 based catalyst were examined and the result shows highest photocatalytic activity of CZA-10.2 was obtained when it was calcined at 600^{0}C (92.5%), over the CZA-10.2 calcined at 500^{0}C (64.31%) and CZA-10.2 calcined at 700^{0}C (84%). Hence, CZA-10.2 based catalyst calcined at 600^{0}C has best photocatalytic performance over degradation of methyene blue.

. Key works: Photocatalysis, Cellulose, Water hyacinth *(Eichhornia crassipes),*

Table of Contents

List of tables

List of figures

Acronyms and abbreviations

XRD……X ray Diffractometer

SEM……..Scanning Electron Microscopy

TEM……Transmission Electron Microscopy

XPS……x-ray photo spectroscope

FTIR……Fourier Transform Infrared ray

BET……Brunauer–Emmett–Teller

LBLD ……Layer by Layer Deposition

CZ……$Zn_{1-x}Cu_xO$

CZ-1……$Zn_{0.99}Cu_{0.01}O$

CZ-2…… $Zn_{0.98}Cu_{0.02}O$

CZ-3……$Zn_{0.97}Cu_{0.03}O$

CZ-4……$Zn_{0.96}Cu_{0.04}O$

CZA……CZ-2/Ag_2O(different percent of Ag_2O)

CZA-6.8……CZ-2/Ag_2O (6.8%)

CZA-10.2……..CZ-2/Ag_2O (10.2%)

CZA-13.6……..CZ-3/Ag_2O (13.6%)

CZA-20.4……..CZ-2/Ag_2O (20.4%)

Z……ZnO

A……Ag_2O

X……Copper concentration, i.e., 0.01, 0.02, 0.03 and 0.04.

MB……Methylene Blue

CHAPTER ONE

1. Introduction

1.1. Background of the study

Now a day textile, pulp, paper, and dyeing industries are, rapidly spreading all over the world, especially in developing countries. These industrial wastewater contains different kinds of dyes like Methylene blue, Methyl orange, Rhodamine B, and so on. These dyes have enormous negative impact on human health and the whole ecosystem [1]. Because of their aromatic nature and complex organic structures, removal of those dyes requires more advanced technology than conventional wastewater treatment methods [2]. However, because of enormous limitations of waste water treatment methods, removing those dyes through an effective, reliable, and eco-friendly way remains as challenge [3]. Advanced Oxidation Process (AOP) is an advanced wastewater treatment technology, which includes Fenton based, Ozon based and Photocatalysis [1]. Among those, the photocatalysis method is the preferred technique. Because it is a green technology, uses naturally renewable solar energy, oxygen from the air, and operates under ambient pressure and temperature [4].

Photocatalysis is the most fundamental form of research and applicable technique for wastewater treatment, self-cleaning glass, and other applications. Fujishima and Honda discover the water splitting phenomena through the utilization of Titania (TiO_2) electrode under ultraviolet (UV) light irradiation [5], Semiconductor photocatalysis technology become an attractive field of study from efficiency, cost and environmental point of view [2]. Semiconductor materials such as TiO_2, ZnO, SnO2 and CeO_2 act as Semiconductor photocatalysts, however, ZnO is the most efficient due to its high stability, low cost, nontoxicity, large photoelectric conversion efficiency and manageable material under ultraviolet (UV) light spectral region [7-9]. However, the UV light content of solar light reaches the earth's surface is only about 5% and visible light is about 48%, therefore we need to harvest the larger portion (i.e., visible light) for better efficiency. However, ZnO's wide band gap energy (3.37eV) , narrow visible light absorption, the high

recombination rate of the photo-generated electron-hole pairs limits its photocatalytic application under visible light. [3]. Hence the synthesis of ZnO with an enhanced visible light response, high specific surface area, and low recombination rate are the major research concerning areas. To solve these problems, different researchers have been focused on designing heterogeneous photocatalysts [10]. Additionally, several types of research tried to enhance the light absorption range and inhibit the e-/h+ recombination rate of ZnO semiconductor through different methods [11]. Including, doping and forming of P-n heterojunction with lower bandgap semiconductors are the most common techniques [12-14]. For example, according to most research reports [15-18], doping with copper is the best technique to improve its photocatalytic activity because of its unique interaction properties with ZnO [19, 20]. Moreover, several p-type semiconductors with a low bandgap have been coupled with ZnO such as, CdS [21], ZnSe [22], In_2O_3 [23], and CuO [24], Ag_2O [25]. Among them, Ag_2O, p-type semiconductor becomes a recent promising candidate for the designation of heterojunction with ZnO semiconductor because of its narrow band gap of 1.2eV and facile preparation [26]. However, Cu-doping on ZnO and formation of Ag_2O/ZnO only may not be effective and sufficient for photocatalytic activities from surface area and high visible light point of view. Hence, it is beneficial to design active and porous catalysts for efficient absorption of visible light sources [27].

Bio–template synthesis technique is the very recent and most effective way of using biological renewable resources. This could provide a more porous structure, because of the unique heretical and complex nanostructural features of the biological sources [28]. Hence, different porosity improved reports have been made on ZnO and TiO_2 by using these biological renewable resources like cellulose, lignin, and Chitosa as scaffolds [29]. Accordingly, cellulose is reported to have the best capacity to act as a scaffold for the synthesis of nanostructure materials because of its unique surface properties such as the existence high hydroxyl group [30]. For instance, Zehao Lin et al., fabricated a series of hierarchical natural cellulose template Ag_2O-nanoparticle/TiO_2-nanotube nanocomposite with enhanced photocatalytic activity on the degradation of Methylene blue, Rhodamine B and norfloxacin [3]. Gajanan Kale et al., synthesized Cu-doped zinc oxide (Cu–ZnO) nanostructure using Whatman filter paper as a template trough combustion method with enhanced photocatalytic activity on the degradation of methylene blue (MB) [4].

Most common cellulose sources have been reported to be commercially available filter papers, bacteria, and plants [3,31,32]. Except for plants, these sources have negative effects from cost and safety points of view [33]. On the other hand, using different plants as the cellulose source is also ineffective from deforestation's point of view. Therefore, finding an appropriate and safe source for cellulose extraction is also another challenge for the bio-template research area.

Water hyacinth with a scientific name *Eichorniacrassipes* locally called 'Emboch' is a very recent spreading weed plant in a water environment. Owing to its high absorption property, it is a dangerous kind of plant for the survival of water bodies [34]. Their rapid spreading and their surviving ability in water surfaces for a long time made them difficult to control [35]. On the other hand, Water hyacinth is reported to be one of the potential cellulose-containing natural weed plants, with a chemical composition of 8% hemicelluloses, 17% lignin, and 60% cellulose. [36]. Therefore, the mention reference works on Cu-ZnO articles have limitations from the e^-/h^+ recombination and low visible light absorption point of view. On the other hand, ZnO/Ag2O photocatalysts based articles have limitations from their surface area and visible light absorption point of view, Hence, there was no report on cellulose extracted from water hyacinth used as a template for photocatalytic or other purposes and there was no report on the synthesis of metal-doped ZnO/Ag_2O composite with cellulose extracted from water hyacinth as a template for the photocatalytic degradation of organic dyes.

Herein, we report the synthesis of $Zn_{1-X}Cu_XO/Ag_2O$ composite where X=0.01, 0.02, 0.03, and 0.04 trough employing of natural cellulose extracted from water hyacinth as a template. The resulting catalysts were characterized using different characterizing instruments. The photocatalytic activities of CZA were also examined on the degradation of Methylene blue under visible light irradiation. Moreover, the effect of calcinations temperature on the degradation efficiency of CZA (10.2%) was also studied. Finally, the reusability of CZA (10.2%) was studied for three consecutive rounds. Accordingly, the detailed review on worked literatures will be discussed on chapter two, materials and methods on chapter three, result and discussion on chapter four and conclusion with recommendations will be discussed on chapter four.

1.2. Problem of statement

Now days, the rapid development of industries is introducing a large amount of organic pollutants into natural resources of water. Among them, organic dyes are the most dangerous components discharged form textile, paper, pulp, and dyeing industry effluents which may cause severe environmental and health problems [5]. To solve these problems, semiconductor photocatalysts have been used extensively for the removal of organic dyes from industrial wastewater [38]. Among them, ZnO is reported to have higher efficiency in the photocatalytic performance due to its high electron mobility [39]. However, the photocatalytic performance of ZnO is limited due to its wide band gap energy (E_g= (3.37 eV), high electrons and holes recombination rate, low absorption efficiency, and low surface area. Although many researchers tried to solve the limitations to enhance photocatalytic performance of ZnO, further modification is needed to enhance the photocatalytic efficiency on the degradation of dyes. To overcome those limitations, this study proposed a multipurpose solution with the synthesis of Cellulose $Zn_{1-X}Cu_xO/Ag_2O$ for the degradation of methylene blue under visible light irradiation, where X=0.01, 0.02, 0.03 and 0.04. Because, the doping of ZnO by copper is to increase the visible light absorption of ZnO photocatalyst through reducing its band gap in to visible spectral region. Additionally doping with copper was found to be effective from availability, cost effectiveness and less toxicity point of view [6]. And then composite formation of $Zn_{1-X}Cu_XO$ with Ag_2O is to increase the photocatalytic activity of $Zn_{1-X}Cu_XO$ photocatalyst through reducing the electron-hole recombination. Cellulose as a template by using an unwanted plant called water hyacinth as a source of cellulose could enhance the surface area by increasing the porosity of the composite catalyst.

1.3. Objective of the study

1.3.1. General objective

Synthesize cellulose templated $Zn_{1-X}Cu_XO/Ag_2O$ composite photocatalyst for the degradation of Methylene blue under visible light irradiation.

1.3.2. Specific objectives

- To extract Cellulose from Water hyacinth, by using conventional method.
- To Synthesize of undoped-ZnO, Ag_2O, cellulose templated $Zn_{1-X}Cu_XO$, where X= 0.01, 0.02, 0.03 and 0.04, and cellulose template $Zn_{1-X}Cu_XO/Ag_2O$ composite.
- To optimization of synthesized $Zn_{1-X}Cu_XO/Ag_2O$ composite by varying the concentration of Cu to be doped and concentration of Ag_2O to be loaded on the photocatalytic degradation of Methylene blue.
- To examining the reusability (Stability) of the optimized $Zn_{1-X}Cu_XO/Ag_2O$ catalyst
- To check the calcinations temperature effect on the optimized $Zn_{1-X}Cu_XO/Ag_2O$ catalyst for photocatalytic degradation of Methylene blue

1.4. Scope of the study

This research work started with the collection of water hyacinth and extraction of its cellulose. Then, the synthesis of cellulose templated $Zn_{1-X}Cu_XO/Ag_2O$ composite catalysts for the photocatalytic degradation of Methylene blue under visible light irradiation was the main objective. To enhance the photocatalytic performance of the catalyst, the optimization with varying the amount of Cu and Ag_2O was performed. The effect of Calcination temperature and pH on the degradation of organic dye was also examined. Finally, the reusability of the catalyst with higher performance was studied for three consecutive runs.

1.5. Significance of the study

It is well known that most of the heavy duty industries are planted at the country sides. And then, most of the people around county side utilize that wastewater from those industries, which contain a lot of hazardous organic dyes for human being and the land itself. On the other hand, water hyacinth is dangerous plant for the survival of large water bodies and removing water hyacinth is a hot issue in our country, Ethiopia. In additional to these, it is also well known that, Africa's geographical location is at the equator of the earth. Therefore, a large amount of sunlight reaches to the earth's surface as a source of safe and renewable type of energy. If this study successfully hits its goal on the real world application, it will be a promising solution for the mentioned problems through removal of organic dyes from industrial waste water under visible light irradiation using cellulose as a template, which is extracted from unwanted plant water hyacinth. Consequently, the beneficial of this work will be different industries and people around the industrial implants. Additionally this work can be used as a benchmark for government from utilizing unwanted plant water hyacinth for useful purpose point of view.

CHAPTER TWO

2. Literature Review

2.1. Introduction

The general sources for wastewater can be classified into two main categories. These are residential sources and non-residential sources [7]. Residential sources are waste waters commonly called 'sewages', which are mostly diluted wastewater composed of 99.90% pure water and 0.10% of residential pollutants such as suspended solids(i.e. Body wastes, food wastes, toilet paper and etc.) , biodegradable organic compounds(i.e. Proteins, carbohydrates, fats and etc.),Inorganic solids (i.e. sediments, salts, metals and etc.), nutrients (i.e.,nitrogen and phosphorus) and pathogenic microorganisms [7]. Non-residential sources are waste waters that are discharges from different heavy duty industries, agricultural parcels, various commercial institutes and rain. The composition of these waste waters include different heavy metals and organic dyes from different industries, harmful chemicals and biological pollutants such as pesticides and fertilizers from different agricultural fields, different kinds fatty stuffs and grease from restaurants and also rain carries different organic and inorganic contaminants from different avenues[8].

Now days, expeditious increment textile industries results a large amount of different types of organic dyes. These dyes results enormous kinds of serious health defects [8]. Owing to these, different methods were applied to remove those dyes from different textile industry wastewater residuals. From those methods, convectional wastewater treatment methods were the primary and common methods, these are: filtration, flocculation, and activated charcoal and ion exchange resins [9-12]. However, these conventional methods are not effective on industrial wastewater treatment especially for the removal of organic dyes, because they only convert the form of pollutant, from one type of pollutant into another. That means, during their treatment the adsorbed pollutant from liquid effluent is converted in to a solid adsorbent [13]. Thus, the solid adsorbent by itself becomes new pollutant which requires further treatment. On the other hand, organic dyes have aromatic structural nature, that need further chemical reaction to break the bond [14]. Hence, researchers on this area are continuously searching efficient, reliable and ecofriendy methods to remove those dyes and treating industrial waste water [15]. Advanced

Oxidation Process (AOP) remove pollutants thorough complete mineralization and converting them in to carbon dioxide and water through the aid of strong radicals (i.e., *OH and O_2^-*) [13]. These radicals are produced through several process via AOP; such as, ozone based processes, Fenton based processes, photocatalysis and so on [1, 16-18]. From them, photocatalysis method is the preferred teqnique, because it is a green technology, uses naturally renewable solar energy, oxygen from air and operates under ambient pressure and temperature [13]. Since Fujishima and Honda have discovered water splitting using Titania (TiO_2) electrode, semiconductor photocatalyst become research concerning area for treatment of industrial wastewater trough photocatalytic degradation of organic dyes [3, 19] .

Generally, in this section, we reviewed different ZnO photocatalyst enhancement based research works on the degradation of different organic dyes under visible light irradiation. Thus, we have tried to review different recent research works on the band gap engineering methods to shift the spectral absorption of ZnO in to visible region. We also tried to review various research works with inhibition of e-/h+ recombination and enhancing their surface areas trough increasing their porosities. On the mid while, we have tried to identify some research gaps from their environmental, cost effectiveness, reliability and performance point of view.

2.2. Photocatalysis

Photo-catalysis is the most promising industrial wastewater treatment technology. This advanced technology uses light active catalysts as an intermediate in order to degrade corresponding toxic pollutants from contaminated water [20]. Currently, owing to its unique properties and cost effectiveness, photo-catalysis become a target technique for many researchers as a promising method for environmental issues and energy rectification [5]. Photo-catalysis is such a gifted method, because, it can be used for different applications. Some of these applications are degradation of different kinds of organic pollutants from waste water, hydrogen production and antibacterial activities[21, 22]. From all of its application, wastewater treatment application of photo-catalysis method becomes attractive research area.

Basically photo-catalysis process is divided into homogeneous photo-catalytic process and heterogeneous photo-catalytic process [23, 24]. Most of the time, in the presence photons the

metal ion complex with high oxidation radical generate hydroxyl group which in turn react with different kinds of toxic organic pollutants and finally destroy them [23]. Because of their supportive assembly of their electronic structure with filled valance band and empty conduction band and unique properties such as high charge transport properties with light absorption capabilities, Heterogeneous photo-catalytic process is applicable on semiconductor nanomaterials (TiO_2, ZnO, SnO_2, and CeO_2) and they are called semiconductor photo-catalyst [25, 26]. In the next section, the working principle of hetrogeneous photocatalyst will be revised.

2.2.1. Working principle of semiconductor photo-catalyst

The performance of photo-catalytic reactions are basically depends on available light energy and the catalyst involved. Generally, semiconductor materials are the candidate materials for photocatalytic reactions because of their electronic structure and unique properties as mentioned earlier. The working mechanism and fundamental steps are mentioned in Figure 2.1. As shown in the Figure 2.1, the light energy in the form of photons fall down on the surface of the semiconductor catalyst; when the band gap energy is equal or greater than the semiconductor band gap energy, electrons will be ejected in to the conduction band of the catalyst semiconductor from the valance band of the given semiconductor and the holes will be remained at the valance band [5].

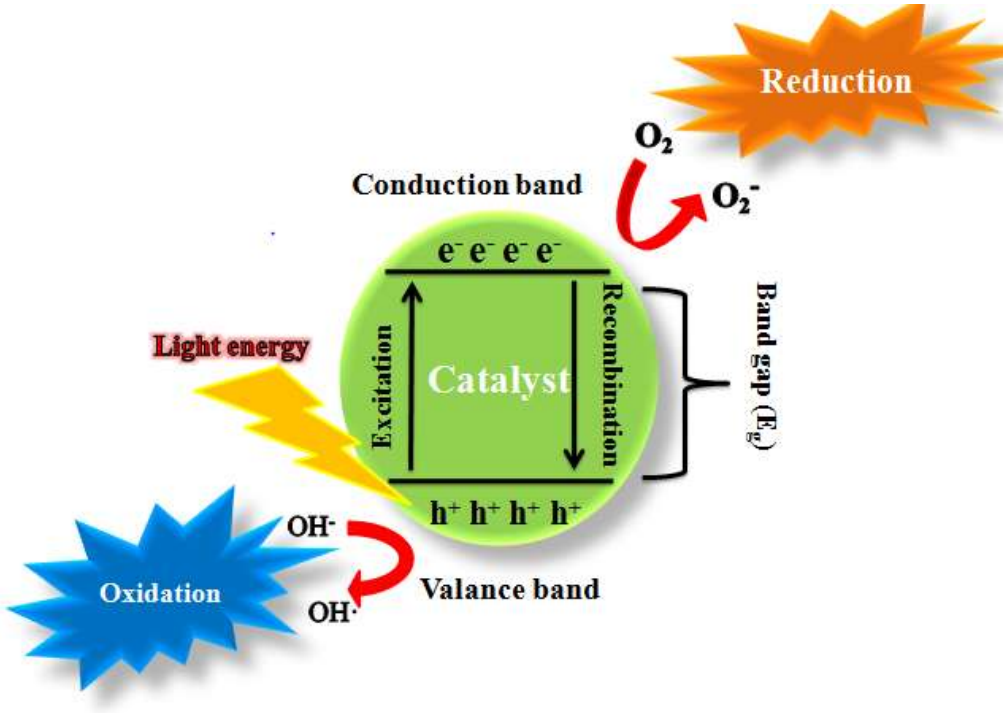

Figure 2.1. Schematic representation for semiconductor photocatalytic working mechanism.

The remaining holes at the valance band will oxidize the surrounding water in order to form hydroxyl radicals. These hydroxide radicals have strong capacities for degradation of toxic pollutants, so that, they react with organic pollutants present in dyes and decomposes them to carbon dioxide and water, this process is the Oxidation process, as shown in the Figure 2.2 [27].

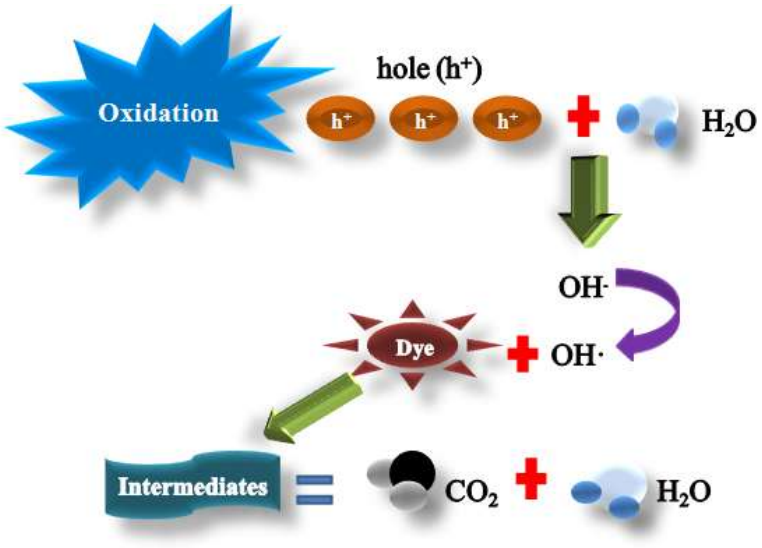

Figure 2.1. Schematic representation of oxidation mechanism

As shown in Figure 2.3, the electrons at the conduction band will react with dissolved oxygen in order to form superoxide ions. These superoxide anions undergo a series attachment to the intermediate products that are produced in oxidative reaction, as a result peroxide will be produced or will be changed to hydrogen peroxide and then to water. This process is called reduction process and it is more easily occur in organic compound than in water [28].

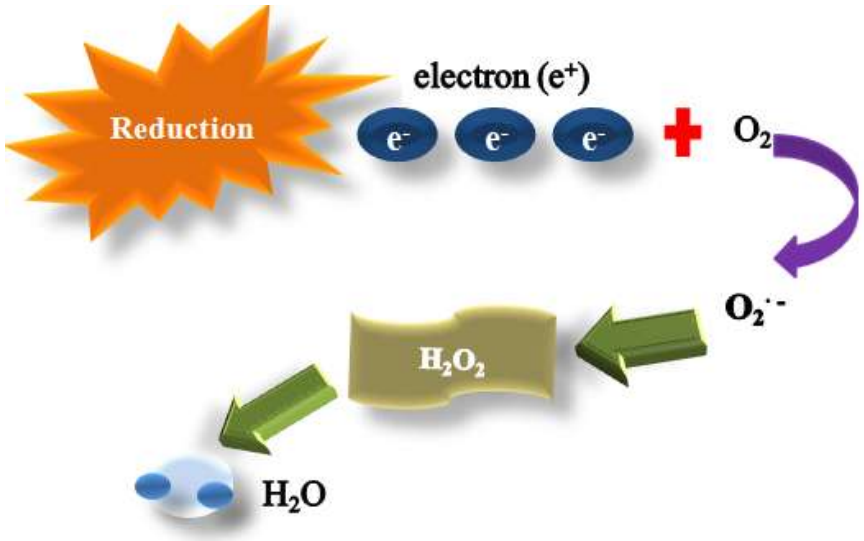

Figure 2.2. Schematic representation of reduction mechanism

2.2.2. Affecting parameters of photocatalysis process

The performance and rate of the photo catalysts depends on different affecting parameters. Some of such affecting parameters are: structure, shape, size, and surface area of the semiconductor catalyst; reaction temperature, pH value, intensity of light, amount of catalyst, and concentration of treated wastewater [28-31].

The structure of the given catalyst plays a fundamental role on the efficiency of the given catalyst by affecting the photo catalytic activity of the photo catalyst whether it is positive or negative effect. For example in TiO_2 semiconductor case, from the three phases such as anatase, rutile and brookite phase, anatase phase is the most stable phase with hydroxylation and high adsorption capacity [32, 33]. The other most influential affecting parameter is the morphology of the catalyst and this directly affect the degradation capacity of the catalyst [34-36]. According to Saravanan et al. report that spherical-shaped ZnO samples show higher efficiency compared with the spindle-and rod-shaped ZnO samples due to its large surface area [37].

Nanomaterials with high surface area and smaller size have higher photocatalaytic efficiency than bulk materials[38, 39]. As the size of the catalyst become smaller, a large number of atoms can be assembled on the surface of a catalyst, this will increase the surface to volume ratio. Owing to this property, the number of active sites and interfacial charge carrier transfer rates will be enhanced; so that the photocatalytic activities will be improved [38]. In photocatalytic reaction, the photocatalytic redox reaction m takes place on the surface of the catalyst ; so that the surface properties mainly play a significant role on the final efficacy of the catalyst [32, 40].

A lot of researches have been reported the effect of reaction temperature on the photocatalytic activity of the photocatalyst [41-43]. In the case of TiO_2 catalyst, when the reaction temperature is above 80^0c, the electron- hole recombination rate will be enhanced; so that the photocatalytic efficiency will be diminished. Owing to photonic activation, heat is not needed for photocatalytic reactions so that it can operate at room temperature. As reports of different researchers, the optimum reaction temperature range for photocatalytic activity of TiO_2 catalyst is to be in the range of 20–80 °C [44].

In the case of photocatalytic reactions, the pH value of the solution is plays a great role on the efficiency of the catalyst. As Shourong et al. research report, the change in pH value affects the efficiency of degradation capacity of the catalyst both on ZnO and TiO_2 photocatalysts [45, 46]. Different results of photocatalyst research results clearly shows the lower degradation efficiency in the acidic solutions (pH < 5), this is because as the concentration of the protons increases, the degradation of the dye is inhibited. But, in alkaline medium (pH > 10), the photo degradation reaction will be improved as the hydroxyl ions defuses the acidic end products that are produced. But when the pH value comes to 12-13, the degradation shows a little decrement. This is because of the rapid scavenging of hydroxyl radicals (OH); so that they cannot react with the dyes [32, 47].

Another kind of affecting parameter is light intensity; which is also another fundamental affecting parameter for photo catalysis reaction. The wavelength of light source is also affecting parameter for the final product of photocatalytic reaction [32, 41]. In most of photocatalysts

including TiO_2, photocatalytic reaction rate depends on the square root of light intensity above a certain value of the intermediate value of light intensity. At high value of light intensity, a lot of electron-hole recombination will be happened; so that the photocatalytic reaction rate is going to be diminished [44, 48].

The amount of the catalyst is also another affecting parameter as it influences the final degradation efficiency of photocatalytic reaction. When the amount of catalyst increased, the number of active sites where the reaction held on will be increased; so that the amount of OH and O radicals also increased which enhances the degradation efficiency of the photocatalyst [40, 48]. In the next section, semiconductor photocatalysts and their modifications will be reviewed.

2.3. Semiconductor photocatalyst

Most of semiconductors are promising candidate for the current nanotechnologies for different applications; especially photovoltaic and phocatalyst applications. But, not all semiconductors are suitable for photocatalyst process. Some of the criteria's are stated for choosing of the appropriate semiconductor materials for photocatalyst applications. Among these criteria, the candidate semiconductor materials should have appropriate band gap (i.e. ranging from 1.7ev to 3.2ev), high light absorption capacity, and efficient charge carrier mobility, precise band edge position, non-toxicity, bio compatibility, and chemical stability.

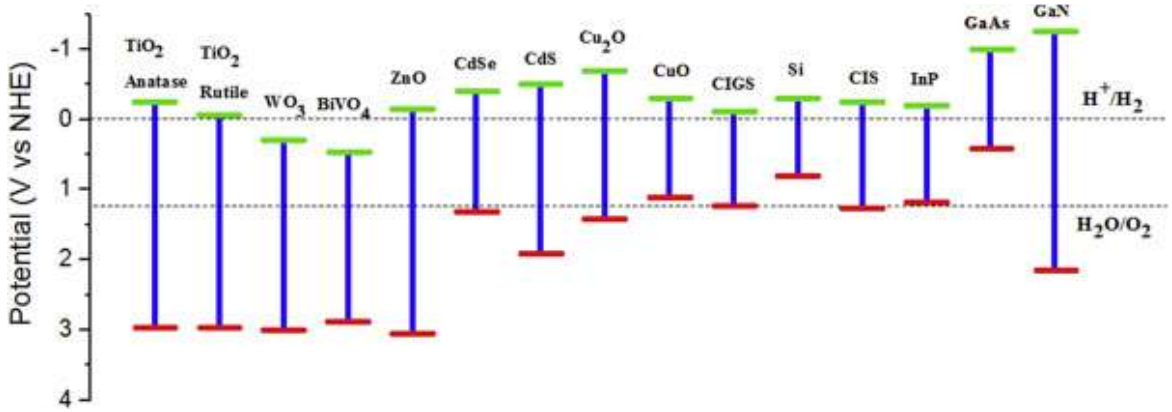

Figure 2.3. Band edge positions of some semiconductor photocatalysts[49].

However, single semiconductor photocatalyst are not effective from photoinduced electron- hole recombination point of view. Accordingly, this appropriate semiconductor photocatalysts are classified in to binary metal oxide compounds, chalcogenides ternary compounds and quaternary

compounds based on their band alignment [50]. As shown in the Figure 2.4, different semiconductor photocatalyst have different band edge positions, this determines their possible band alignment for their photocatalytic application. Accordingly, ZnO and TiO_2 based photocatalysts are the most common and effective photocatalysts. However, ZnO based photocatalysts are reported to have high photocatalytic performance over TiO_2 on the degradation of organic dyes, because of their good optoelectronic, low cost, non-toxicity, good catalytic and photochemical properties [6].

2.4. ZnO Based Photocatalysts

The most important features of the photocatalytic system are the appropriate band gap, surface porosity, high surface area, high stability, and recyclability of the given catalyst [51, 52]. The photocatalytic performance of ZnO is limited because of its large band gap energy (3.37eV), narrow light absorption, high recombination rate of the photo-generated electron–hole pairs, and poor adsorption capacity [3]. Due to this reason, different researchers dig out a lot of modification mechanisms in order to enhance the photocatalytic performance of ZnO photocatalyst [53]. Accordingly, Several research groups have focused on different methods to improve the photocatalytic efficiency of ZnO photocatalyst [54]

2.5. Mechanisms to enhance photocatalytic performance of ZnO

Herein, those modification teqniques are categorized in to three main categories. These are band gap engineering, Coupling and selection of appropriate synthesis methods. From band gap engineering point of view, different researchers focused on doping. Doping mainly modifies (narrow) the band gap and coupling or forming heterogeneous p-n junctions enhances the separation of charge carriers in addition to its ability to enhance the visible light absorption capacity [54]. On the other hand, surface modification techniques have been experienced through utilization of different template in order to increase their porosity [55]. Finally, the selection of appropriate synthesis methods for the formation of catalysts was evaluated from their reliability, environmental and cost effectiveness point of view [56]. The detailed information about different research reports regards these methods are mentioned in the following sections.

2.5.1.1.1. Band gap engineering

From energy and environment point of view, efficient consumption of sunlight as a source of energy is very essential [53].The spectral composition of solar light that reaches to the surface of the earth consists of 5% of ultraviolet(UV) spectral region (300-400nm), 43% of visible light spectral region (400-700nm) and 52% of infrared spectral region (700-2500nm) [57, 58].It is known that ZnO photocatalyst have wide band gap energies of 3.37. Accordingly, its optical absorption lies on the ultraviolet (UV) spectral region which takes a very small portion of solar light [59]. Owing to this, different researchers dig out a lot of band gap engineering techniques in order to improve the photocatalytic efficiencies of the ZnO semiconductor in order to let them to be active in the visible light spectral region [49, 53]. Some of the common techniques in band gap engineering involve doping, Co-doping, coupling with narrow band gap semiconductors, and crystal anisotropic growth. Among them the most effective techniques are doping and coupling of ZnO with narrow band gap semiconductor.

2.5.1.1.1.1. Doping

The main purpose of doping is to modify the large band gap of semiconductors and electronic structure. In order to enhance the optical properties to be active on visible light region, improving charge kinetics to diminish recombination rate and enhance the interface and surface properties of semiconductors are important [60]. The same is true for ZnO semiconductor. the Doping ions offer additional energy levels that aid to trap electrons or holes as separate carriers for successful diffusion in to the surface of ZnO semiconductor [60]. Doping by itself is divided in to non-metal doping [61, 62], transition metal doping [63, 64], self doping [65, 66], and rare earth metal doping [67, 68].

Doping with non-metals

Non-metal elements that have high ionization energies and high electron affinity are candidate non-metals for enhancement of photocatalytic performance of ZnO semiconductor in visible light region by narrowing the band gap and shifting its absorption edge in to visible light region. The common non-metals are boron [69, 70], nitrogen [71, 72], carbon [73, 74], sulfur [75, 76], fluorine [77, 78] and chlorine[79, 80]. Doping of ZnO semiconductor with these non metals successfully narrows the band gap of the corresponding semiconductors [81]. C, N, and S, are more efficient in increasing the visible light absorption capacity because they can form

intermediate energy levels in band gap of ZnO of ZnO, Figure 2.6 [82]. From them, C-doped ZnO indicate even greater extent of light absorption than others, because, after C doping, the new band forms slightly below the VB top; this shifts the hole bands to downward position. [83]. For instance, Yu. W.jzhang et al., reported a high visible light absorption of C-doped ZnO over pure ZnO, N-doped and S-doped ZnO [83]. Similarly, Ch et al., synthesized C-doped ZnO nanomaterials with high visible light absorption and efficient degradation of orange II dye.

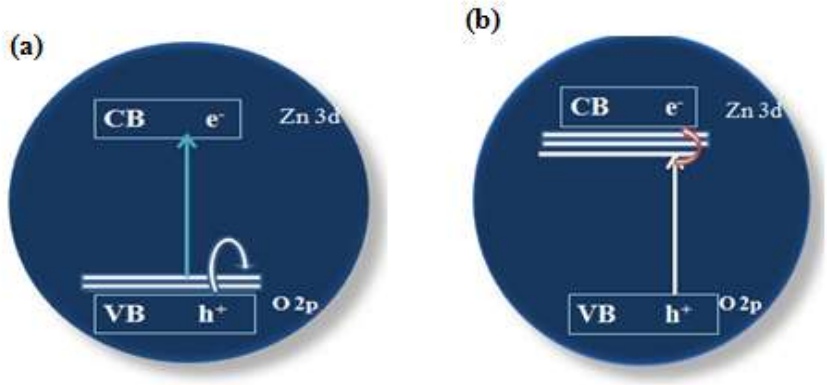

Figure 2.5. Schematic representation of (a) non-metal doping and (b) metal doping

Even though, those non metal dopants have similar atomic radius with oxygen atom, they don't have similar atomic radius with Zn atom; hence doping them to ZnO become difficult. In addition to that, the reliability of those non-metal dopants are limited from their health, Cost, environment and availability point of view. [50, 84]. Therefore, different authors suggest metal ion doping or co-doping for better photocatalytic activity [85-88].

Doping with Metals

Addition of selected cation dopants will tune the optical, structural, electrical and chemical properties of ZnO. This phenomena is also true for enhancing the photocatalytic performance of the given semiconductor photocatalyst including ZnO [51]. Doping with metal will enhance the performance of ZnO through the addition of group I, group V and transition metals elements [89, 90]. According to most research reports, among metals, doping with transition metals is the best technique to improve its photocatalytic activity because transition metals and their cations possess an unfilled d and f orbitals and change the electronic band structure, and induce large amount of defects (i.e., oxygen vacancies) in to lattice structure [91-94] [95]. Their main purpose

is attributed to creating oxygen vacancies, that act as electron taps between the band gap of ZnO; this mainly improves the charge separation efficiency of e−/h+ [96, 97]. From them, transition metals with similar atomic radii to that of Zn can be easily doped into the ZnO lattice [98]. Accordingly many transition metals, with similar atomic radi with ZnO have been doped to ZnO to narrow its band gap; to let it to be active on visible spectral region. These type of transition metal dopants that had used so far include Fe [99], Co [100], Ni [101], Mn [102], Cr [103], V[104], Cu [105], and Zr [106]. However, the type and concentration of the dopant transition metals are the main factors affecting the photocatalytic performance of the doped ZnO. Accordingly, doping of ZnO with Fe, Cr, Co, Ni and Mn, is not prefable because their solubility limits are high, they need more concentration to revamp their modification on ZnO (up to 25-35 at. %) [84]. Therefore, doping of ZnO with transition metal like Cu or Ag is more preferable because of their low solubility limit (below 2-5 at. %) [107]. However, from cost effectiveness and availability point of view, doping with Cu is more preferable than Ag. Additionally, copper is relatively affordable element and its atomic size is nearly similar to Zn, so that Cu^{2+} can easily enter in to the lattice structure of ZnO as a substitution ion in order to modify the absorption and emission spectrum of ZnO into visible-light spectral region [108]. This modification is due to the installment of localized 3d states of Cu in the band gap of ZnO [109].

Table 0.1: Overview of transition metal doped ZnO photocatalysts under visible light irradiation

Dopants	Synthesis method	Bandgap narrowing	Pollutant degraded	Source of light	Reference
Cr	Solvothermal	365nm-400nm	azo-dye	Visible light radiation	[92]
	Wet chemical	3.2ev-2.9ev	Methyl blue	Natural sun light	[110]
V	Sol-gel	386nm-420nm	Organic pollutants	Sunlight	[111]
Mn	Solvothermal	375nm-485nm	OrangeII dye	Solar light Irradiation	[112]
	Wet chemical	3.2ev-3.1ev	Rhodamine B (RB)	300W Xenon lamp	[102]
Mo	Sol-gel followed by	3.1ev- 3.0ev	Methyl blue	Visible light	[113]

	solvothermal			radiation	
Fe	Co-precipitation	3.2ev-2.8ev	Methyl orange	100W Halogen lamp	[84]
	hydrothermal	3.2ev-2.9ev	Para-nitro phenol	Natural sun light	[114]
Ag	Sol-gel	3.2ev-aroun 2.7	Methyl blue	Perlcin Elmer lambda 35	[115]
Cu	Wet-chemical	3.06ev-3.02ev	Methyl blue	Sunlight irradiation	[116]

There are many reports on Cu-doped ZnO for different photocatalytic applications [109, 117-119]. .Pawar *et al*., [117], Successfully synthesized Cu-doped ZnO and reported that Cu ions doping enhanced the photo-catalytic performance of ZnO microstructures for photo-decomposition of organic pollutants from industrial waste water.V.Vaniano*et al.,* [118] reported the enhanced photo-catalytic activity of Cu-doped ZnO nanoparticles for photocatalytic oxidation of As (III) to As (V) under visible light irradiation. Mohan *et al.,*[109]was also used Cu-doped ZnO nanorod with enhanced photocatalytic performance, through vapor transport synthesis method for the degradation of resazurin dye. Jognavavakit *et al.,*[119] also successfully synthesized Cu-doped ZnO nanoparticles with improved photocatalytic performance. According to Mittal, M., et al., ZnO crystal will shrink in order to confirm the substitution of Cu^{2+} as a result, Cu-doped ZnO shows more intense PL spectra than pure ZnO [120]. Unlike other transition metals, as the concentration of Cu increases, the band gap decreases. For instance, Mittal, M., et al, synthesized Cu-ZnO and their results shows that as the concentration of Cu dopant increases from 1to 5 at%, the band gap keep decreasing [120]. However, as Vaiano et al., reported, the solubility limit of Cu in ZnO lattice was limited to 5 at%; above that limit additional Cu atom or CuO phases will be observed. In addition to this, Cu-doping also enhances the morphology in order to increase the specific surface area where the photocatalytic reaction takes place. For instance, Polat et al., successfully produce Cu-doped ZnO with rod shape morphology on glass substrate through chemical bath deposition synthesis technique for the

degradation of methylene blue [109]. Their result shows that, as the concentration increases from 1-3 at%, the change in morphology happens from paramedical shape to hexagonal rod shape morphology; which increases the surface area of reaction and enhances the photocatalytic performance [109]. Despite of dopant copper ions has outstanding capacity in inhibiting the e-/h+ recombination rate, they are not that much good enough on narrowing of band gap deep in to the visible light irradiation spectrum [121]. Hence, different researchers have been focused on hetrojunction designing of ZnO semiconductor with another narrow band gap semiconductor

2.2.4.1.1.12. Coupling (Heterojunction)

Visible light responsive hetrojunction catalyst is another technique is one of modification technique for making catalyst active in visible light region[122]. Type II p-n junction is the best technique because of the synergetic effect of the both semiconductors, for narrowing of the band gap to be active to visible light region and to suppress the recombination rate through formation of depletion region between them.

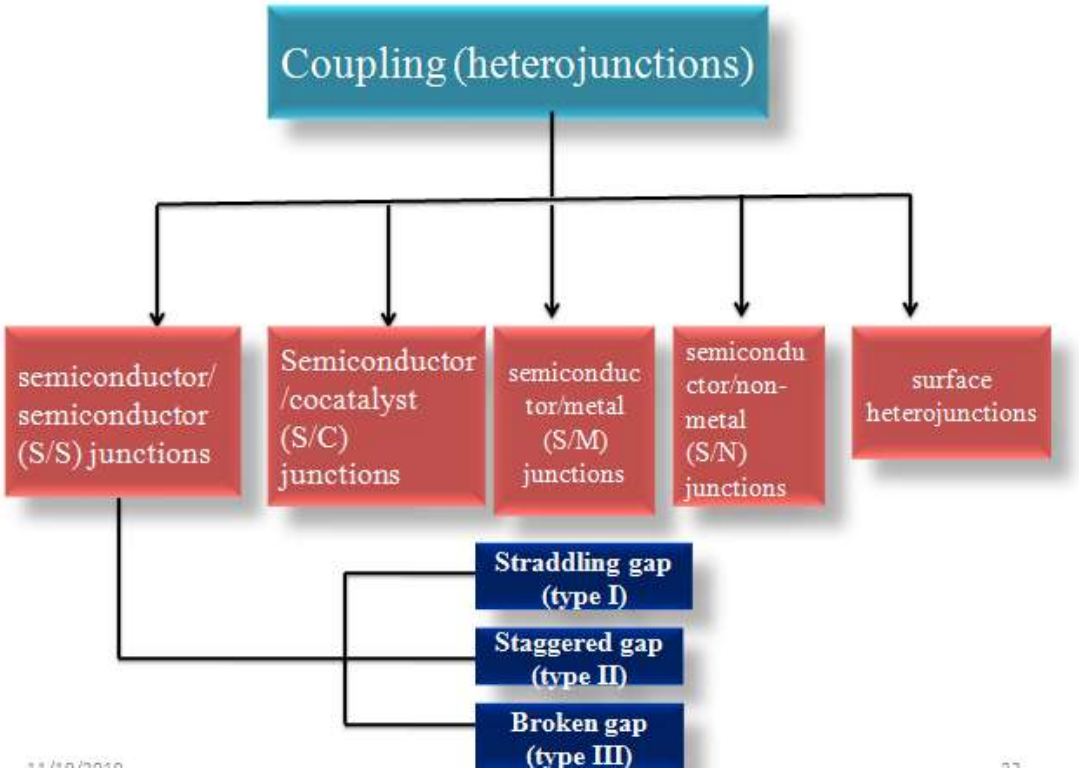

Figure 0.6. Schematic representation for classification of hetrojunction

2.5.1.2. Semiconductor/semiconductor junction

These types of junctions are classified in to three main categories based on the band arrangement. These are: type I (straddling gap junctions), type II (staggered gap junctions), and type III (broken gap junctions). Recently, type II is the most promising arrangement for enhanced separation of photo generated electrons and holes. Based on the mechanism of charge separation and charge separation between the contact semiconductors, there are three types of junctions: n-n junctions, Z-scheme junctions and the most efficient one p-n junction [122]. Among these, p-n junction will be discussed in detail in the following section.

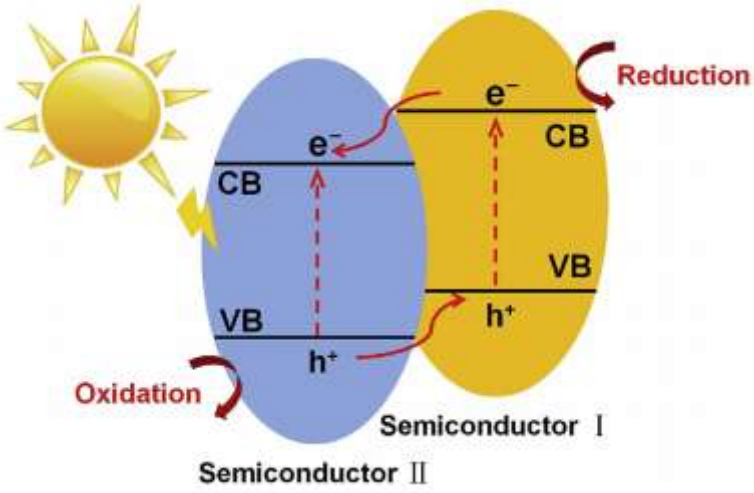

Figure 0.7. Schematic representation of type II p-n hetrojunction [123].

The purpose of strategically formation of p-n junction through combination of narrow band gap p-type semiconductor with wide band gap n-type semiconductor (e.g., TiO_2 and ZnO) , is not only shifting the light absorption edge from UV spectral region to visible light spectral region, but it is also inhibits the photo generated electron- hole recombination. As ZnO is an n-type semiconductor, several p-type semiconductors with a low band gap have been coupled with ZnO. For instance, CdS [124], ZnSe [125], In_2O_3[126], and CuO [127], Ag_2O [128].

Among them, silver oxide (Ag_2O) is one of the most stable narrow band gap semiconductor with band gap energy of 1.2 eV and with small atomic radii Ag_2O has high photocatalytic performance under visible light irradiation [129]. When compared to other narrow band semiconductors (ZnS and CdS), photo corrosion behavior of Ag_2O is balanced by relative

instability of AgO and binding energy of Ag [129, 130]. According to reports, the p-type-Ag_2O/n-type-ZnO heterojunction structure narrows the band gap and provide enhanced photo-catalytic performance under visible light irradiation[131]. For instance, Jing Wang *et al*., [128] successfully synthesized Ag_2O/ZnO micro-flowers heterostructure with enhanced photocatalytic performance under visible light irradiation. Abjhit*et al*., [132] synthesized Ag_2O/ZnO nanocomposite as highly efficient visible light active photocatalyst for photo-detoxification of methyl orange. However, still it is challenging task to get high performance Ag_2O/ZnO with unique structure that could enable to have more active sites and large surface area for the enhanced photocatalytic degradation of organic dyes and other pollutants with different molecular structure.

2.5.2. Template mediation

Template mediation teqnique is another technique of enhancing the photocatalytic performance of heterogeneous photocatalyst by increasing its surface area. Biotemplate synthesis of these heterostructure provides a significant solution for those problems mentioned above by providing natural, unique, heretical and complex nano structural features by introducing natural bio-substance in to artificial substance [55]. As a result, the synergetic advantages from biomass substrates and introduced gust components provide a significant solution to solve porosity problem that could not be solved by using only artheficial constituents for the current advance technology[133, 134].

Natural polymers resulted from waste products or renewable resources can be used as a promising organic template for inorganic semiconductor metal oxides [135]. Some of them are Polysaccharides, lignin, cellulose, hemicelluloses, chitin, chitosan, starch, which hold excellent biodegradability with high specific surface area and can be used as natural templates for the synthesization of photocatalytic hybrid nanocomposite[136]. These natural polysaccharides possess high swelling capacities and low resistance to ultimate wastewater conditions (i.e., acid medium), this may causes significant leaching; consequently, those natural polymer based catalysts cannot be stable and may cause organic matter expansion in wastewater. Therefore, using natural polymers as a template or support is more advantageous [137]. The sources of these Natural polymers are mainly wood, plants or residues of different living organisms [138-140].

The natural fibers derived from those natural polymers are mostly used as reinforcements or as a support for different composite materials because of their recyclability, ecofrendiness, higher volume fraction and larger loading capacity over synthetic polymers [141, 142]. Accordingly, they are broadly utilized as a template for the formation of composite materials more of photocatalysis filed.

2.5.2.1. Lignin templated ZnO and TiO_2 based photocatalysts

Due different linkages that connect the phenyl propanoid-based units, lignin has a complex structure [143]. Therefore, they can be used as a stable biopolymer support for different composite materials [144]. For instance, X chen et al., synthesized lignin templated mesoporous TiO_2 nanoparticles through hydrolysis precipitation synthesis method with enhanced high surface area (i.e., 165.8 m^2 g^{-1} and a pore volume (i.e., 0.312 cm3 g−1) [144]. They also have adsorptive properties for the elimination of inorganic compounds from polluted aqueous solutions [145].However, its extraction is time consuming and they need high annealing temperature to remove them out. [146].

2.5.2.2. Chitin /Chitosan templated ZnO or TiO_2 based photocatalyst

Chitin is the second most aboundant natural polysaccharide and chitosan is obtained from partial deacetylation of chitin [147, 148]. Chitosan can be used as an absorbant for the elimination of organic contaminents because of its enourmous functional groups. Owing to this, chitosan have high specific surface area in its fiber or bead form. Therefore, chitosan have high adsorption capacities [149]. They can also be used as a template for different photoctalysts to give them herarical structure and increase their surface area. For instace, G. Xiao et al., [150] have showed the enhanced photocatalytic efficiency of core–shell Chitosan supported TiO_2 hybrid material (SICT) on the degradation of methyl orange. Colmenares et al., synthesized surface imprinted TiO_2/Chitosan Comosite using chitosan as a scaffold or support; their generalized procedure is shown in the Figure 2.8 [151].

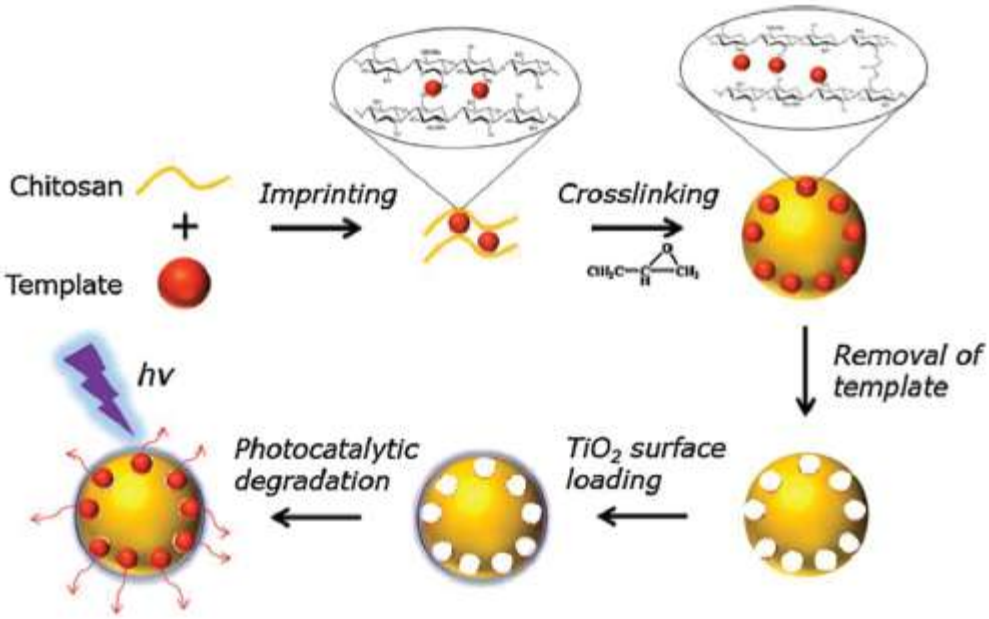

Figure 0.8. Schematic representation of the synthesization process of the surface imprinted TiO2/chitosan composite [151].

Furthermore, chitosan was used as a template because of its easy recovery and reusability, comfortable for selection of target contaminants, overall degradation of organics and this synergistic phenomenon of the adsorption–photocatalysis processes of TiO_2/chitosan leading to enhancement of photocatalytic efficiency trough lowering of the charge carrier recombination [151]. However, the disadvantage of this chitosan as a support or template for enhancing the specific surface area is that its requires special fabrication method , i.e., electrospining [152].

2.5.2.3. Cellulose template ZnO or TiO_2 photocatalyst

Cellulose is the best one due to its hierarchically cross linked three dimensional structure and surface property with abundantly contained with hydroxyl groups, so that, coating other guest components in the form of ultrathin films on the surfaces of the cellulose is absolutely possible[3]. Furthermore, plant cellulose fibers have relatively low annealing temperatures; therefore, it is possible to use low-temperature synthesis techniques. (e.g., sol-gel methods, precipitation method, hydrothermal method, and dip coating method, etc.) coat on such cellulose fibers [153].Accordingly , the cellulose substance is capable to be utilized as a template or scaffold for the synthesis of nanostructure materials[154]. For the fabrication of such cellulose

templated well-designed hetrojunction nanocomposite, the layer-by-layer (LbL) self-assembly technique is believed to be the most effective and common synthesis method [155-158].

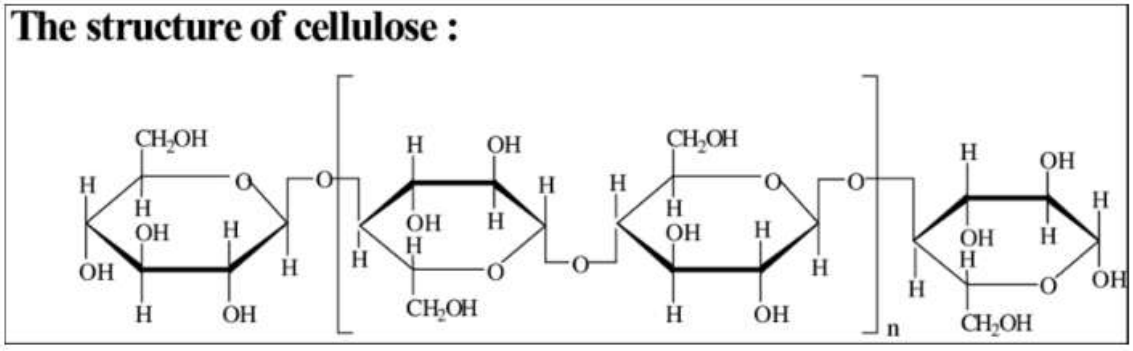

Figure 2.9. Chemical structure of cellulose [159].

Recently, different researchers focused on this research area. For instance, Yu et al. synthesised cellulose-templated TiO_2/Ag nanosponge composites for the degradation of of RhB with improved photocatalytic performance [160].Zehao Lin et al., fabricated a series of hierarchical natural cellulose template Ag_2O-nanoparticle/TiO_2-nanotube nanocomposites with enhanced photocatalytic activity on the degradation of methylene blue, Rhodamine B and norfloxacin [3].Gajanan Kale et al., synthesized Cu-doped zinc oxide (Cu–ZnO) nanostructure using Whatman filter paper as a template trough combustion method with enhanced photocatalytic activity on the degradation of methylene blue (MB) [4].

However, the synthesis of cellulose templated heterostructure was rarely reported [161-163] Therefore, further work regarding this productive research area is still required. On the other hand, the source of the cellulose is also another concentrating area. Some of common cellulose sources have been reported to be commercially available filter papers [3], different types of bacteria sources, and plants with their different parts[4, 151, 164, 165]. However, except plant, these sources have negative effect from cost and environment point of view. On the other hand, using plants as a source of cellulose also have negative effect from deforestation point of view. They may also have another additional disadvantage; therefore it is better to use dangerous or unwanted plant as a source of cellulose for photocatalytic or other purpose. Accordingly on this work, we used unwanted plant called water hycthin as a source of cellulose as a support.

2.6. Water hyacinth (Eichorinia crassipes)

Water hyacinth with a scientific name Eichornia crassipeslocally called 'Emboch' is a very recent spreading weed plant in water environment. Under appropriate growth environment, water hyacinths can double their number in just one week and they can also survive in water for continuous six years, this make water hyacinth difficult to control [166]. Therefore, it is very challenging current topic to remove this type of plant for the survival of water resources of our country as well as the whole world [167]. So that different authorized bodies are working on the possible solutions to solve this problem. However, most of the solutions applied to solve this problem are creating another additional problem for the water bodies due to the addition of toxic ingredients to remove water hyacinth from water bodies[168].

Figure 2.10. Image for Water hycthin (Koka Lake, Ethiopia)

On the other hand, Water hyacinth is reported to be one of potential cellulose containing natural fiber weed plant. As it is strong fiber plant, it can be used as reinforcing agent in different composites [167]. As reported by Abdel the chemical composition of Water hyacinth is about 8% hemicelluloses, 17% lignin and 60% cellulose [169].

CHAPTER THREE

3. Materials and Methodology

3.1. Chemical reagents

Zinc nitrate hexahydrate ($Zn(NO_3)_2.6H_2O$) (Loba Chem, 99%,), Copper nitrate trihydrate ($Cu(NO_3)_2.3H_2O$) (Sigma Aldrich, 99%), Silver nitrate ($AgNO_3$) (Loba Chem, 99%), Sodium hydroxide (NaOH), Metaylene Blue (MB), ethanol, and sodium chlorite were purchased from Loba Chemical Reagent Company. All of the chemicals were analytical grade. All aqueous solutions were prepared using distilled water.

3.2. Collection and preparation of Water hyacinth

Water hyacinth for this experiment was collected from 'Koka Lake', which is 22.8 Km far from 'Adama' town. Then, the collected water hyacinth was washed with distilled water, dried for three consecutive days in drying oven at 60 ^{0}C, grinded and stored at room temperature for the next experiment.

3.3. Extraction of Cellulose

The grinded water hyacinth powder was dewaxed with the solution of 2:1 (v/v) mixture of toluene/ethanol for 6 h for the purpose of removing the wax constituent. The dewaxed powder was bleached and boiled with 3% of sodium chlorite solution under acidic condition. The suspension was maintained for 3 h at 80 ^{0}C and allowed to settle over night. The process was repeated twice, washed with distilled water until free from acid. The hemicelluloses were removed from obtained tissue by treating with 1 wt% of sodium hydroxide solution at 60 ^{o}C for 24 h. The samples were centrifuged and washed with distilled water. The lignin was removed by further treatment with 1 wt% of sodium chlorite solution under acidic condition and stirred well at 75 ^{o}C for 48 h. The samples were centrifuged and washed with distilled water. The remaining hemicelluloses was removed and resulted to pure cellulose fibers by treating with 5% of NaOH solutions at 55 ^{0}C for 24 h with continuous stirring. Finally, the obtained residues was centrifuged and washed with distilled water till free from alkali [167]. The schematic representation of the main procedures are shown in Figure 3.1.

.

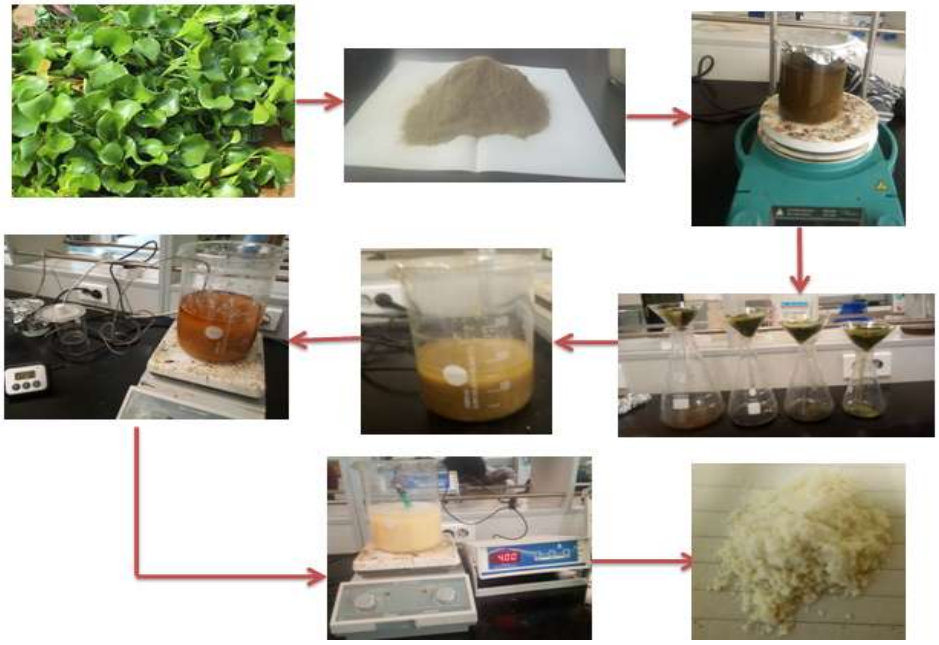

Figure 3.1: Schematics for Extraction of Cellulose from Water hyacinth

3.4. Preparation of photocatalyst

3.4.1. Synthesis of $Zn_{1-x}Cu_xO$ particles

$Zn_{1-x}Cu_xO$ based catalysts, where, (x= 0.01, 0.02, 0.03 and 0.04) were synthesized through green co-precipitation method using cellulose as a template. 0.5 g of cellulose was mixed with 100 mL of distilled water under stirring for 10 min for homogenization purpose. Then, 0.1 (1-x) M of (Zn $(NO_3)_2.6H_2O$), and 0.1x M of Cu $(NO_3)_2$. $3H_2O$ were added to the above solution. Then, the mixed solution was stirred under magnetic stirrer for 1h to form the aqueous solution and assigned as (solution A). On a mid while 2 M of NaOH was dissolved in 100 mL of distilled water under magnetic stirring 5 min to form the aqueous solution and assigned as (solution B). Then, (solution A) was added into (solution B) drop by drop until the pH value of the solution reached to 10.35. The obtained precipitate was centrifuged and washed with distilled water and ethanol to remove the residuals, followed by draying in oven at 80 ºC for 24 hr. Finally, the obtained powder was calcined at 600 ^{0}C for 2 hr to get the desired $Zn_{1-x}Cu_xO$ based catalysts [170]. Cellulose templated ZnO and bare ZnO, $Zn_{1-x}Cu_xO$ catalysts were synthesised via the same procedure for comparison purpose.

3.4.2. Synthesis of $Zn_{0.98}Cu_{0.02}O/Ag_2O$ composite catalysts

$Zn_{0.98}Cu_{0.02}O/Ag_2O$ based composite catalysts were synthesized through simple co-precipitation technique. Firstly, 100mg of $Zn_{0.98}Cu_{0.02}O$ powder was added into 2.5 mL of distilled water and dispersed with sonication for 30 min. Then, 15 mg of $AgNO_3$ (10.2% of Ag_2O) was dissolved in another 2.5ml of distilled water and dropped in the $Zn_{0.98}Cu_{0.02}O$ dispersed solution and continuously stirred for 30 min. Then after, 10 ml of 0.06 M of NaOH was dropped under continuous stirring for about 10 min. Consequently, the resulting powder was collected by centrifugation, washed, and dried at 80^0C for 24hr. The resulting composite catalyst was abbreviated as CZA-10.2. Similarly, different amounts of $AgNO_3$ (i.e.,10 mg, 30 mg and 45mg) were loaded on $Zn_{0.98}Cu_{0.02}O$ paricles and abbreviated as CZA-6.8 (6.8% of Ag_2O), CZA-13.6 (13.6% of Ag_2O) and CZA-20.4 (,20.4% of Ag_2O) respectively. Furthermore, bare Ag_2O particles were synthesized with 20 mg of $AgNO_3$ with the same procedure without adding $Zn_{0.98}Cu_{0.02}O$ particles for comparison purposes.

3.5. Characterizations

The chemical bonds and functional groups of the synthesized cellulose from water hyacinth and other samples were determined by using FTIR instrument (Ft/IR-6600 type A). Examining of the morphology of each sample and the elemental composition were characterized by Scanning Electron Microscope (SEM) and Energy Dispersive analyzer (EDS) (COXIEM-30). Determination of the crystal structure of phases of each sample was characterized by using X-ray Diffraction instrument (XRD) (XRD-7000S Shimadizu). The optical properties and catalytic performances of samples were examined by using UV-vis spectroscopy (UVvis-3600plus Shimadzu).The thermal property was investigated by using Thermal Analysis Technique (DTG-6OH Shimadizu). Photocatalytic performance of each sample will be examined under visible light irradiation by using 150W Halogen lump.

3.6. Photocatalytic experimental set-up

Photocatalytic experiments was conducted as follows using related research paper as a reference [171]. Typically, 25 mg of catalyst was added in to 125 mL of MB solution. The solution was sonicated for 30 min in the dark to reach the equilibrium of adsorption and desorption between the surface of the catalyst and the dye. The mixture was stirred using magnetic stirrer during all of the experiments. Consequently, the solution was irradiated under the visible light illumination. Every 20 min time intervals, an aliquot were withdrawn from the system. Before analysis, the photocatalyst was separated from the solution by centrifugation. Each measurement was performed by replica. A control run without the involvement of catalyst was used as reference. The degradation of MB dye was analyzed through measuring the change in absorption intensity at λ under visible light spectral range. Furthermore, the effect of pH values on the photocatalytic activity of CZA-10.2 was performed by adjusting the pH of the solution to 3.5 and 11.5 by using HCl and NaOH respectively.

CHAPTER FOUR

4. Result and Discussion

.

3.7. Characterization of Synthesized CZA catalysts.

4.1.1. X-ray diffraction (XRD) analysis

XRD diffractometer was used to analyze the phase purity, crystal structure and crystalline size. As shown in Figure 4.1a, the XRD patterns for as- synthesized Z, CZ-1, CZ-2, CZ-3 and CZ-4 samples were examined and the diffraction peaks correspond to (100), (002), (101), (102), (110), (103), (200), (112) and (201) planes at 2θ values of 31.8^0, 34.5^0, 36.3^0, 47.6^0, 56.7^0, 62.9^0, 68.0^0, 69.6^0 and 77.0^0 were perfectly matched with hexagonal wurtzite structured ZnO (ICDD card No.036-1451). However, the enhancement of Cu content causes marginal shift of the identified XRD peaks towards higher angle side (Figure.4.1b). This phenomena is due to the shrinkage of ZnO crystal lattice as a result of the substitution of Zn^{2+} (0.074 nm) by smaller Cu^{2+} (0.072 nm), which confirms Cu^{2+} can easily substituted into the crystal lattice of ZnO [172, 173]. This also shows the decreasing of interplannar distance (d), unit cell volume (V) and Zn-O bond length (L) [121]. This may be attributed to the electro-negativity difference between Zn and Cu (i.e., 1.91 and 1.65 [167, 174], and ionic radius (i.e.,0.74Å and 0.72 Å), respectively [175]. This information is consistence with corresponding data's of our experiment. Many other researchers also confirm the oxidation state of Cu^{2+} from XRD [172, 173] which is similar with our XRD data. There were no additional Cu related phases (i.e., Copper oxides and metallic copper phase) in the CZ-1, CZ-2 and CZ-3 samples: which shows the proper substitution of Zn^{2+} by Cu^{2+} without altering the ZnO lattice structure [176]. However, the addition diffraction peaks observed on sample CZ-4 represents the corresponding XRD diffraction peaks to CuO and lied at around $2\theta = 31^0$ and 39^0 .This result assures the other researcher's results who reported the solubility limit of Cu in ZnO is below 5%. [118]. This information is consistence with similar behavior confirmed by lot of other researchers. Accordingly, they reported that as long as the Cu dopant concentration is kept under stated number, the wurtzite structure will remain as it is [121, 177, 178].

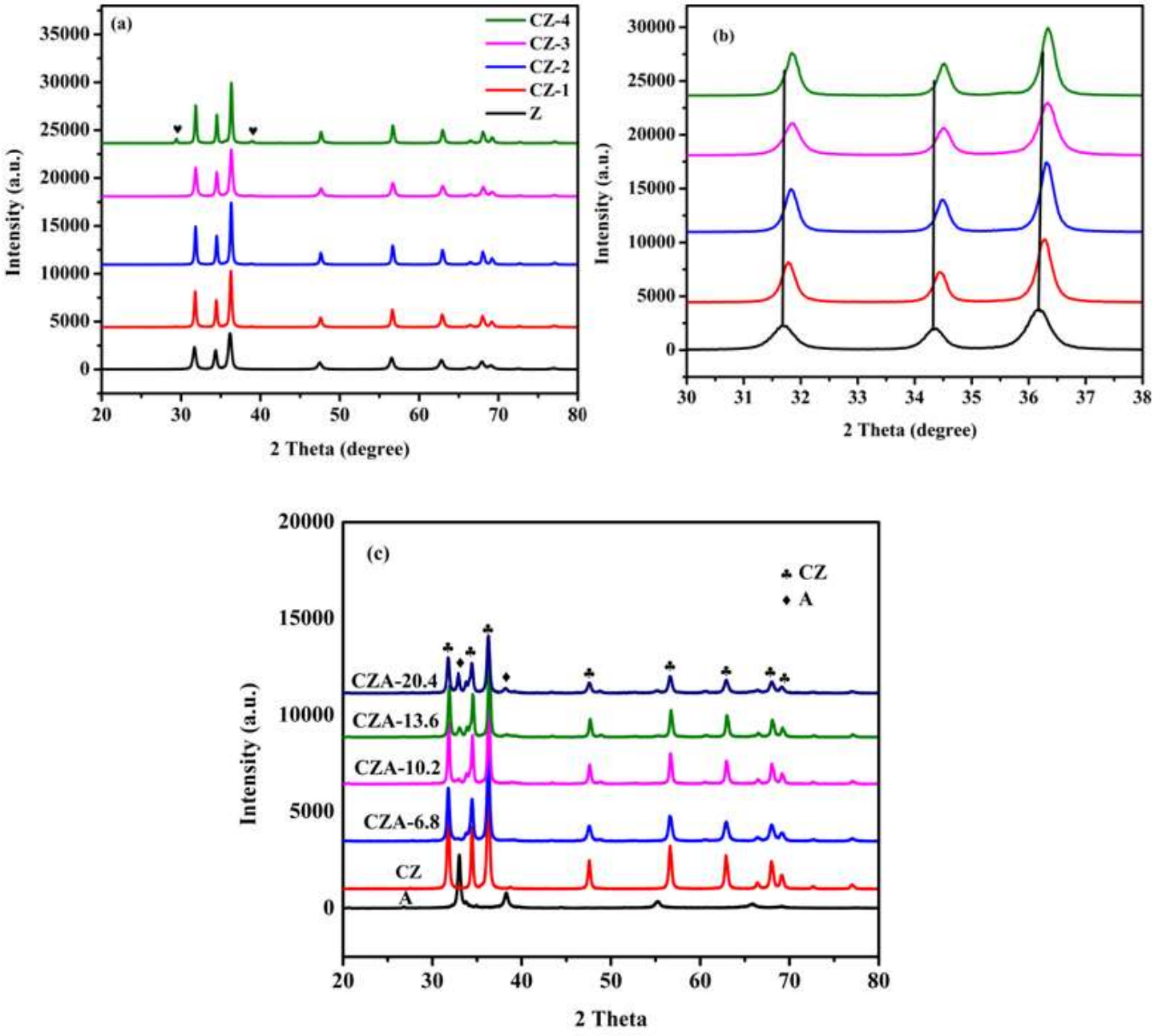

Figure 4.1. XRD diffraction patterns of (a) $Zn_{1-x}Cu_xO$ where, (x= 0.00, 0.01, 0.02, 0.03 and 0.04), (b) and enlarged diffraction peak from 30^0 to 38^0, (c) as- synthesized CZ and CZA samples.

.

As it is shown in Figure 4.1C, the XRD diffraction patterns of the powder samples for CZ, Ag_2O, CZA-6.8, CZA-10.2, CZA-13.6, and CZA-20.4, were characterized. CZ represents CZ-2 from Figure 4.1b. The XRD diffraction patterns of the major peaks of the cubic Ag_2O phase located at 2θ values of 32.2^0, 38.3^0, 55.2^0, and 65.7^0 were observed (ICDDS Card No. 041-1104). Furthermore, the major diffraction peaks for CZ (100), (002), (101), (102), and (110) were appeared with their respective 2θ values of 21.8^0, 34.5^0, 36.3^0, 47.6^0, and 56.7^0. After deposition of Ag_2O particles on Cu-ZnO particles, the XRD peaks that represent Ag_2O were not clearly observed at CZA-6.8 and CZA-10.2. These results indicated the lower amounts of Ag_2O particles and the peaks were dominated by Cu-ZnO peaks. Consequently, as we increased the amounts of Ag_2O (CZA-13.6 and CZA-20.4), the formation of cubic Ag2O were confirmed through additional major peak at 2θ value of 32.8° and 38.3^0. The presence of $Zn_{0.98}Cu_{0.02}$ O and Ag_2O diffraction peaks in the XRD patterns of CZA-10.2, CZA-13.6 and CZA-20.4 together confirms the successful synthesis of the composite catalyst.

According to working principle of XRD, i.e., Bragg's law, the interplanar distance'd' was also calculated as follows

$$2dsin\theta = n\lambda$$

Where 'n=1, 2…, is the wavelength of the incident x-ray beams, $\lambda = 0.89$,'d' is interplannar distance and θ diffraction angle. The crystallite size (D) was calculated from the most intense diffraction peak (101) using Scherer equation by assuming the crystallites were cubic and monodisperse in size [50].

$$D = \frac{k\,\lambda}{\beta_{hkl}\cos\theta}$$

Where k is the shape factor (taken to be 0.89), λ is the wavelength of the incident x-ray beams, β_{hkl} is the full width at the half maximum (FWHM) and θ is the diffraction angle.

Table 1 Represents the values for the average crystallite size (D), diffraction angles (2θ) values and interplanar distance (d) values of each catalyst.

Catalyst	$2\theta^0$	D (nm)	d(nm)
Z	34.088	25.50	0.26290
CZ-1	34.182	26.16	0.26288
CZ-2	34.237	26.29	0.26253
CZ-3	34.237	26.98	0.26244
CZ-4	34.856	39.36	0.26238
CZA-6.8	34.174	32.75	2.62922
CZA-10.2	34.165	32.89	2.62504
CZA-13.6	34.231	33.12	2.62076
CZA-20.4	34.167	34.35	2.62994

From this table we conclude that as the dopant Cu concentration increases from 1% to 3%, (CZ-1 to CZ-3) their crystalline size was nearly similar to undoped ZnO, this implies the correct substitution of Zn^{2+} with Cu^{2+}. However, as the concentration increases to 4% (CZ-4), the crystalline size increases, this may be attributed to the formation of more defects and deformed lattice structure, this is also proved by additional CuO related peak observed in the XRD [179] . On the other hand the crystalline sizes of the composite catalysts such as CZA-6.8%, CZA-10.2%, CZA-13.6% and CZA-20.4%, are almost the same but they have increased crystalline size than the Cu-doped catalysts (CZ-1, CZ-2, CZ-3 and CZ-4). This is attributed to the increment of the diameter of the crystal owing to the formation of composite catalyst.

4.1.2. Thermal analysis

Figure 4.2, shows the TGA/DTA analysis result for Cellulose templated CZ-2 catalyst. In the weight loss journey of Cellulose templated CZ-2 sample four main decomposition steps were observed mainly at three temperature intervals: In the first step (35^0C –200^0C), a small weight loss was observed due to evaporation of moisture from the surface of the sample CZ-2. The second step (331.70^0 - 380.43^0C) represents the minimum weight loss due to pyrolysis decomposition of cellulose and in the third step (380.43 ^{0}C - 430.82^0C) [180]. The small endothermic peak observed at around 430.82 ^{0}C represents mass loss due to full combustion of cellulose, further decomposition of $Cu_2(OH)_3.NO_3$ for the production of CuO and reduction of CuO into Cu metal [181]. As result of these a 14.64% total mass loss is observed on TGA curve. However, after 450 ^{0}C DTA and TGA curve revels the thermal stability of the sample, it shows the complete decomposition of Zinc nitrate hexahydrate and Copper nitrate trihydrate for the formation of Cu-ZnO.

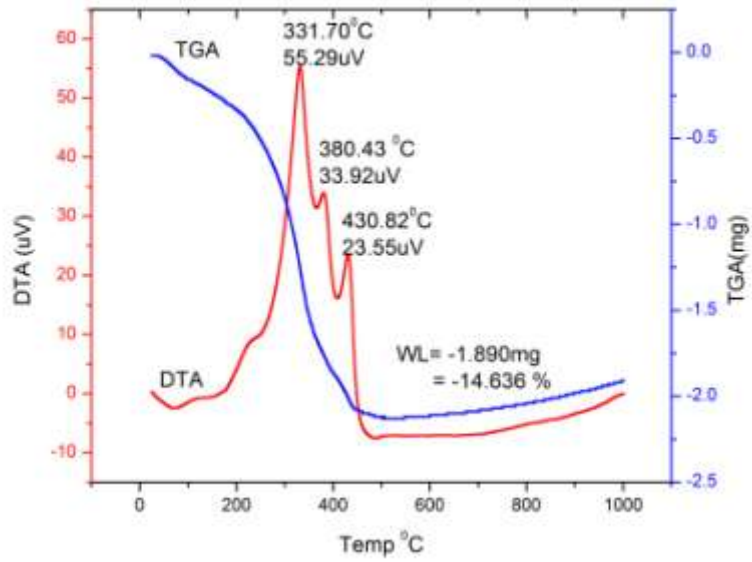

Figure 4.2. Thermal Analysis of Cu-doped ZnO (CZ) catalyst

4.1.3. FTIR Analysis

FTIR spectral analysis was used to obtain detail information about the chemical bonding within the material. Accordingly, the FTIR spectrum of cellulose was analyzed to confirm the successful extraction of cellulose from water hyacinth. Consequently the FTIR spectral analysis was made for uncalcined and calcined CZ-2 catalyst, in order to confirm complete removal of cellulose through the calcinations temperature. Furthermore, the FTIR spectral analysis was made for CZA-10.2, in order to determine the available chemical bonds within the catalyst.

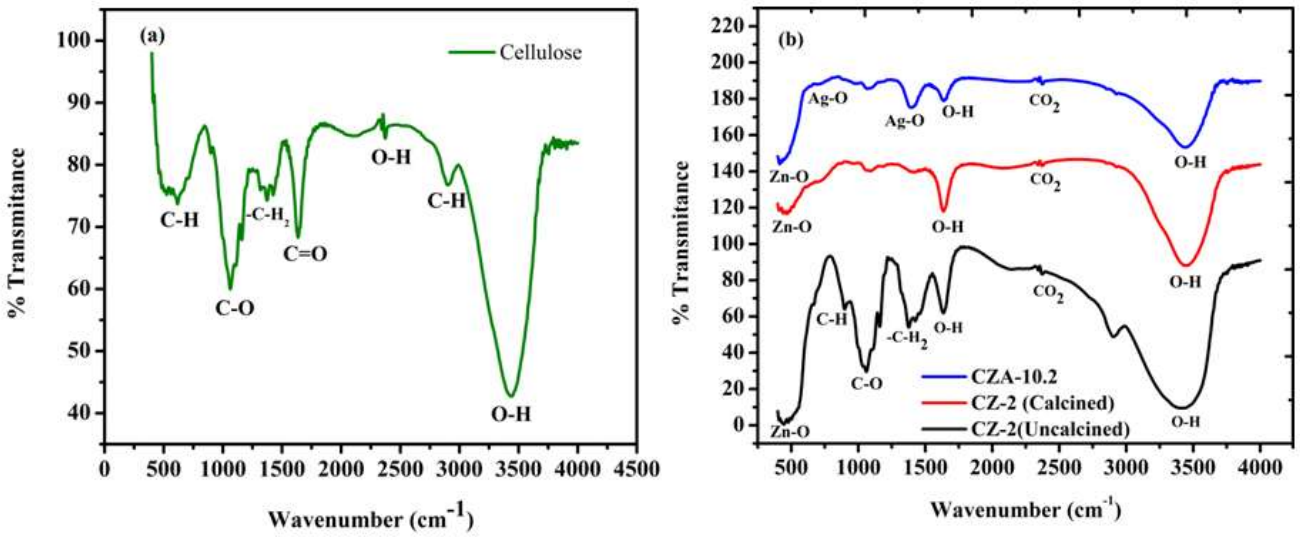

Figure 4.3. FTIR spectra of (a), Cellulose, (b), CZ-2 (uncalcined), CZ-2 (calcined) and CZA-10.2.

As shown in fig 4.3a, the major peaks observed at 3441 cm^{-1}, 2916 cm^{-1}, 2369 cm^{-1}, 1634 cm^{-1}, 1374 cm^{-1}, 1060 cm^{-1}, and 620 cm^{-1} corresponded to O-H, C-H, O-H, C=O, -C-H_2, C-O and C-H stretching bonds respectively [182, 183]. The O-H, stretching bonds may be attributed to the absorbed water on the surface of the cellulose [184]. The other transmittance peaks observed at 2903cm^{-1}, 1060 cm^{-1}, 1374 cm^{-1} and 620 cm^{-1} was attributed to stretching vibrations of cellulose C-H, C-O and –C-H_2 groups respectively [185]. This result confirms the successful extraction of natural cellulose from water hyacinth.

Furthermore, as shown in the Figure.3b, the FTIR spectral analysis was made for uncalcined and calcined CZ-2 catalyst. Accordingly, for uncalcined CZ-2, the transmittance peaks appeared at 884, 1060,1159, and 1381 have the same stretching bonds like cellulose [167]. This confirms the existence of cellulose on the as synthesized uncalcined CZ-2 catalyst. The broaden absorption peaks observed at around 3466 cm^{-1} and 1647 $cm^{-1}$are attributed to O-H stretching vibration of water (H_2O) in Cu-Zn-O lattice structure [186]. This may be due to atmospheric moisture or moisture absorbed on the surface of the catalyst. Moreover, the medium and week transmittance peaks at around 1067cm^{-1} and 738cm^{-1} are owing to the change of microstructure feature of ZnO, due to the addition of Cu in to the Zn-O lattice structure [186]. The %transmittance peaks appeared between 2313cm^{-1} and 2400cm^{-1}, are attributed to the existence of CO_2 molecules in the air [187]. The medium % transmittance peaks at around 464cm^{-1}, 723 cm^{-}1 and 1400 cm^{-1} are expected to be the Zn-O and Ag-O bond stretching [188].

4.1.4. Diffusion Reflectance Spectroscopy Measurement (DRS)

The optical properties of bare ZnO, bare Ag_2O, CZ-2 and CZA-10.2 were determined by measuring their UV–Vis DRS measurement at room temperature in the visible spectral wavelength range of 350–800 nm. In the powder reflection spectra, high reflectance values indicate low absorption values in the corresponding wavelength region [189]. Accordingly, as shown in Figure.4.4a, the reflectance versus wavelength plot for bare ZnO shows higher reflectance in the visible light range (350 nm-800 nm). Therefore, it has a very low, almost insignificance absorption in the corresponding visible light spectral region [118]. However, CZ-2 shows lower reflectance in the visible light spectral region compared to ZnO. This shows enhanced absorption of CZ-2 in the corresponding visible light spectral region. Furthermore, the reflectance of bare Ag_2O shows insignificance amount within visible light spectral region. This shows ultra its high absorption in the corresponding visible light region. Moreover, CZA-10.2 shows lower reflectance than both pure ZnO and Cu-doped ZnO which shows better absorbance of CZA-10.2 catalyst in the visible light range (350-800 nm) from both pure ZnO and Cu-ZnO (CZ-2). On the other hand, it shows lower absorbance than Ag_2O. Even though Ag_2O has higher absorbance in the visible light spectral region, as it is single semiconductor catalyst, there is high electron hole recombination problem, which greatly influence its photocatalytic performance. Therefore, as it is confirmed in the photocatalytic performance analysis, CZA-10.2 catalyst had higher visible light absorption than both ZnO and CZ-2 catalysts.

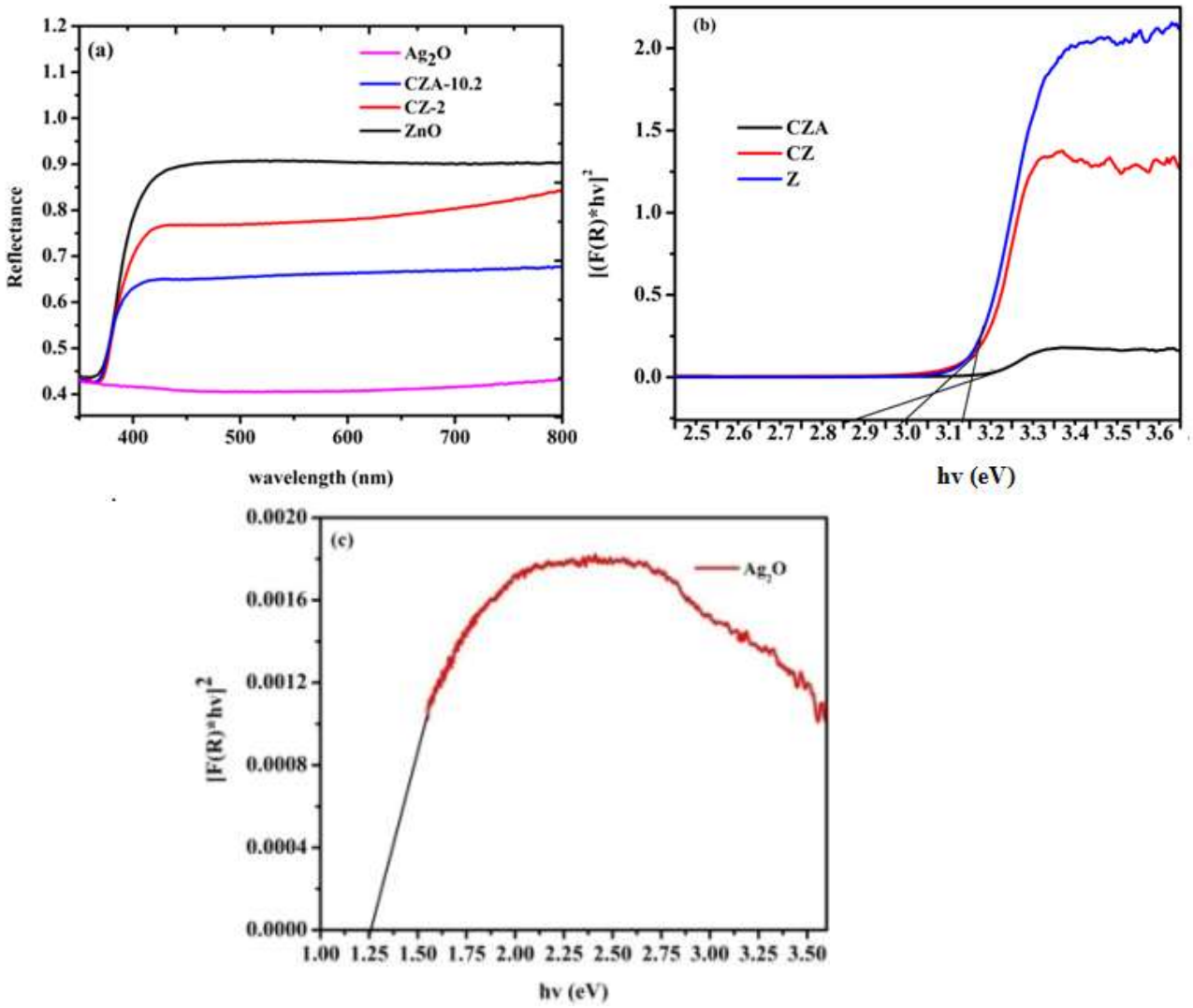

Figure 4.4. Optical properties of Z,CZ-2, CZA-10.2 and Ag_2O on the visible light region (350nm-800nm).

The Kubelka–Munk function was used to calculate the optical band gap value of ZnO, CZ-2 and CZA-10.2

$$F(R) = \frac{(1-R)^2}{2R} \qquad [190]$$

Where, F(R) is the Kubelka–Munk function and R is the absolute value of reflectance.

As shown in the Figure 4.4b, the band gap energy (E_g) of the samples were determined using

Tauc's plot via employing the linear correlation between Kubelka–Munk function F(R) and Eg

$$[F(R).hv]^{\frac{1}{n}} = A(hv - E_g)$$

Where, n=$\frac{1}{2}$, for direct band gap semiconductor materials such as ZnO. Tauc's plot was obtained by plotting a graph between $[F(R).hv]^2$ and photon energy (hv). The band gap of pure ZnO, Ag_2O, CZ-2, and CZA-10.2 were investigated from Tauc's plot through fitting of extrapolation intercept F(R) =0 line were at 3.14, 3.03 and 2.85 eV respectively. Over all, it has been observed that the ZnO (E_g =3.14eV) showed a little absorbance in the visible light region (350nm-800nm), (Figure 4.4b), Ag_2O showed high visible light absorption (E_g=1.26eV) (Figure 4.4c). Thus, the optical shifting of ZnO from UV to visible region was successfully achieved through Cu doping on ZnO (E_g =3.14eV to E_g =3.03eV). This may be attributed to the decrease in Burstein–Moss shifting due to shifting of Fermi level to lower energies as a result of the induced defects during Cu doping [190]. Furthermore, the loading of Ag_2O on Cu-doped ZnO also played a significant role on shifting the band gap of Cu-ZnO in to more visible light region (E_g =3.03eV to E_g =2.85eV); this may be attributed to Band tailing phenomena due to the existence of number of integrated density of states through the whole volume and which results the conduction band states at relatively low potentials and valence band states in relatively high potential regions [190].

4.1.5. Morphology and elemental analysis of CZA

The surface morphological analysis the as-synthesized catalysts was investigated by using SEM. Figure 4.5 a–c shows the morphologies for bare Ag_2O, and CZA-10.2 with and without cellulose respectively. Figure 4.5a, shows the SEM images of bare Ag_2O particles. The CZA-10.2 catalyst without cellulose templated shows nearly diamond shaped morphology (Figure. 4.5b). Moreover, Figure 4.5c, shows rod like morphology for cellulose templated CZA-10.2 and dispersed deposition of Ag_2O particles on the surface of CZA-10.2. According to Figure 4.5b, and Figure 4.5c, the Ag_2O particles were successfully deposited on the surface of CZ-2 with-out aggregation. Therefore, utilization of cellulose as a template for the synthesis of nearly rod shaped CZA was mostly effective. The depositions of Ag_2O particles on the surfaces of both cellulose templated and bare CZA-10.2 composite catalysts were successful. Moreover, the energy dispersive X-ray spectroscopy (EDS) analysis clearly shows the peaks of elements for Zn, Cu, Ag, and O in cellulose templated CZA -20 composite catalyst (Figure 4.5d).

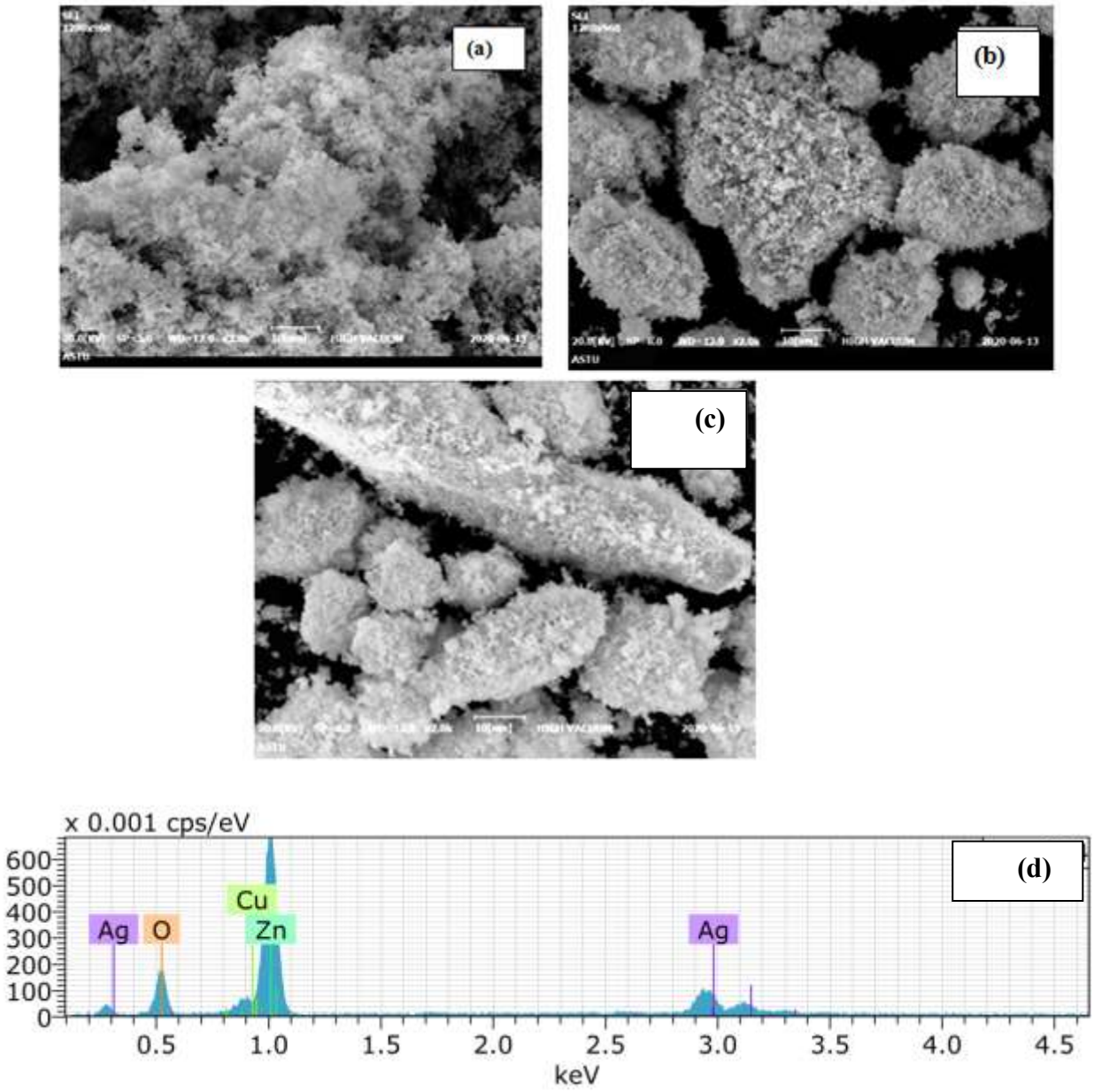

Figure 4.5. SEM image for bare (a) Ag_2O (b) CZA-10.2 with cellulose,(c) CZA-10.2 without cellulose, catalysts, (d) EDS analyses of CZA-10.2 catalyst

4.1.6. Photocatalytic Activities

Methylene Blue dye was the model of organic pollutant chosen on this experiment to check the photocatalytic degradation efficiencies of different photocatalysts with different compositions under visible light irradiation. As shown in Figure 4.6a, Methylene blue had two absorption peaks at 256 and 665 nm and this is also confirmed in other research reports on photocatalytic degradation of Methylene blue [191]. There was no change in Methylene blue concentration without catalyst (blank) under visible light irradiation. Accordingly, Figure 4.6a–d shows the photocatalytic performances of different catalysts on the degradation of Methylene blue under visible light irradiation. The change in concentration of Methylene blue dye with in different interval of time in the presence of CZA-10.2 catalyst is shown in Figure 4.6a. The C_t/C_0 ratio, where C_0 represent the initial concentration of Methylene blue after the equilibrium adsorption and C_t represent the concentration of Methylene blue after visible light illuminated time (t) in min.

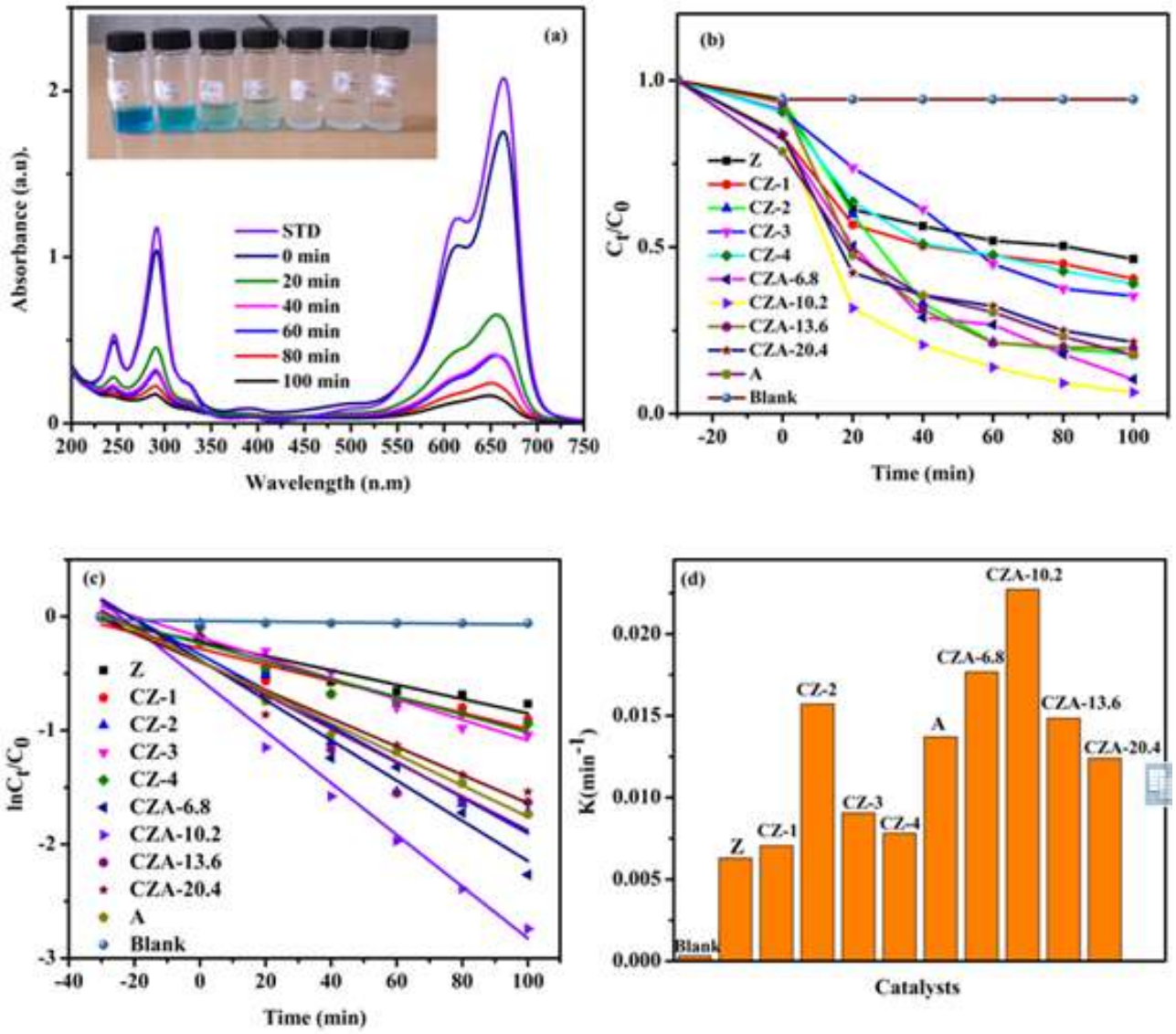

Figure 4.6. (a) UV–vis absorption spectra of CZA-10.2 catalyst after different irradiation times. (b) C_t/C_0 plots, (c) the first-order kinetic plot, and (d) the rate constants of blank, Z,CZ-1, CZ-2, CZ-3, CZ-4, CZA-6.8, CZA-10.2, CZA-13.6 and CZA-20.4 catalysts under Visible light irradiation for different periodic time intervals.

Figure, 4.6b and c, shows the demonstration of the first-order kinetic plot over different samples for the photocatalytic degradation of methylene blue. Moreover, Figure. 4.6d shows the rate constants of the catalysts. As shown in Figure 4.6 b, the degradation of methylene blue without catalyst involvement was irrelevant and its concentration after visible light irradiation for 100 min was unchanged. In the presence of Z about 33.38% of the dye degradation was achieved within 100 min irradiation. Consequently, in the presence of CZ-1, CZ-2, CZ-3 and CZ-4 catalysts, 63%, 82%, 64.59%, and about 60% of the methylene blue was degraded, respectively. Among them, catalyst CZ-2 has highest performance with 82% on the degradation within 100 minute of visible light irradiation, because, as the concentration of the dopant (i.e., Cu^{2+}) increases, there will be large number of oxygen vacancies and act like recombination center [121]. Furthermore, in the presence of CZA-6.8, CZA-10.2 catalysts, the degradation of methylene blue was upgraded to 90.47% and 92.48%. Furthermore, with increasing the Ag_2O content the catalyst degradation percent was decreased to only 79.20% and 79.00% for CZA-13.6 and CZA-20.4 catalysts respectively.

Therefore, the CZA-10.2 (92.48%) composite catalyst showed the best photo degradation efficiency than CZA-6.8(90.47%), CZA-13.6 (79.20%) and CZA-20.4(79.00%) composite catalysts. As we have seen from the data, increasing theAg_2O content will enhance the catalytic activities towards degradation of organic pollutants. However, at much higher Ag_2O content, the photocatalytic performances of the catalyst will decreases. According to other research reports, the reason behind this phenomenon may be attributed to full covering of CZ-2 surfaces by Ag_2O particles [192]. Therefore, 10.2% of Ag_2O content was the limit of the Ag_2O content loaded on Cu-ZnO for is CZA-10.2. Furthermore, the photocatalytic performance of both CZA-13.6 and CZA-20.6 was limited to 79%; this confirms further addition of Ag_2O content of 13.6% and above had no significance on the improvement of the photocatalytic degradation of $Zn_{0.98}Cu_{0.2}O$.

On the other hand, the photodegradation efficiencies of the individual n-type ZnO and p-type Ag_2O oxides were found to be ineffective. However, $Zn_{1-x}Cu_xO$ where x= (0.01, 0.02, 0.03 and 0.04) had better photodegradation efficiency than pure ZnO. Among them $Zn_{0.98}Cu_{0.02}O$ had best photodegradation efficiency due to high visible light absorption. Moreover, n-type CZ-2 and p-type Ag_2O were much better due to the formation of the p–n junction that can decrease the

electron-hole recombination rates [132]. Therefore, the kinetic studies of Methylene blue degradation under visible light have been discussed in the absence of a catalyst, presence of as-synthesized Z, A, CZ-1, CZ-2, CZ-3, CZ-4, CZA-6.8, CZA-10.2, CZA-13.6 and CZA-20.4 catalysts.

According to Langmuir–Hinshelwood (L–H) model [193] the rate expression at low initial concentration is given by;

$$\ln (C_t/C_0) = - kt$$

Where, C_t is concentration of the dye at time t and C_0 is the initial Concentration of the dye, k is the apparent first-order rate constant [194]. A plot of ln C_t/C_0 *versus* time for methylene blue dye photodegradation is shown in Figure 4.6c with different photocatalyst. Accordingly, The photocatalytic degradation reaction for this experiment was confirmed to follow pseudo-first-order kinetics, because of the linear relationship between ln (C_t/C_0) and their respective irradiation time [195]. The rate constants (k) and the values of regression coefficient (R^2) of this experiment for the photo degradation of methylene are listed below (Table 4.2.).

Table 4.2. The rate constants (k) and regression coefficient (R^2) of as-synthesized catalysts with different amount of Cu dope and different amount of Ag_2O loaded under Visible light irradiation.

Catalyst	**K (min^{-1})**	**R^2**
Z	0.000630	0.85857
CZ-1	0.00705	0.89252
CZ-2	0.01572	0.91361
CZ-3	0.00906	0.95972
CZ-4	0.00782	0.93307
CZA-6.8	0.01768	0.96401
CZA-10.2	0.02273	0.96304
CZA-13.6	0.01485	0.89166
CZA-20.4	0.01240	0.92680
A	0.01371	0.97956
Blank	0.00032	0.32723

The values of regression coefficient (R^2) values of this experimental runs were more than 0.86, which indicates that the degradation of methylene blue satisfactorily followed pseudo-first-order kinetics. On the other hand for the first optimization, the rate constant (k) of the CZ-2 catalyst was 25 times higher than that of Z, 2.3 times higher than CZ-1, 1.7 times higher than CZ-3 and 2

times higher than CZ-4. Thus, this result indicated that the degradation efficiency of the CZ-2 catalyst to methylene blue is much higher than those of Z, CZ-1, CZ-3 and CZ-4 catalysts under visible light irradiation. For the second optimization, the rate constant (k) of the CZA-10.2 was 14.5 time higher than CZ-2, 1.7 times higher than A, 1.3 times higher than CZA-6.8, 1.5 times higher than CZA-13.6 and 1.8 times higher than CZA-20.4. The general result confirms that the photo degradation efficiency of the CZA-10.2 composite on methylene blue is much higher than those of CZ based catalysts and CZA composite based catalysts under visible light irradiation.

Degradation mechanism

The possible photodegradation mechanism of Methylene blue dye is illustrated in Figure 4.7. When the p-type Ag_2O semiconductor [196] is connected with n-type Cu-ZnO semiconductor [190], there will be carrier concentration gradients, therefore, the holes diffuse from p-type to n-type region and electrons diffuse from n-type to p-type region and then a p–n heterojunction is formed at the interface [49]. During the photocatalysis reaction, the photogenerated electrons can move to the conduction band of the n-type Cu-ZnO and holes can move to the valence band of the p-type Ag_2O, due to the existence of less barrier between the formed CZA heterostructure [132]. The internal electric field of p–n heterojunction and the band alignment between Ag_2O and Cu-ZnO greatly facilitate the electron–hole separation. Therefore, the photodegradation results reveal that the CZA heterojunction photocatalysts showed the higher photocatalytic activity than as-synthesized CZ, ZnO and Ag_2O photocatalysts.

Both Cu-ZnO and Ag_2O could be exited to generate photo induced electron hole pairs under visible light irradiation, Eqs. (1) and (2). Therefore, the amount of photoinduced electron-hole pairs could increase due to more visible light absorption in both sides. The photogenerated electrons (e-) have an ability to shift from the conduction band (CB) of Ag_2O to the CB of Cu-ZnO Eqs. (3), then trapped by oxygen to form superoxide radical anions (O_2^-) Eqs. (5). simultaneously, the holes (h+) are expected to gather at valence band (VB) of Cu-ZnO moved to the VB of Ag_2O, Eqs. (4) And expected to react with OH^- part from H_2O to produce reactive oxygen species (**.**OH) Eqs. (6). ·OH and ·O_2^- are the foremost active species that decomposed Methylene blue solution [197, 198] Eqs (7) and (8). Therefore, Cu-doping enhances the visible light absorption of ZnO and loading of Ag_2O on the surface of Cu-ZnO will further increases its visible light absorption and reduces the electron hole pair recombination [132]. Hence, for this

experiment as all of the above characterization methods confirmed, both doping of n-type ZnO with Cu and forming of p-n heterojunction with p-type Ag_2O simultaneously could enhance the degradation of Methylene blue under visible light irradiation.

$$Cu - ZnO + hv \rightarrow e^{-}(CB_{Cu-ZnO}) + h^{+}\ (VB_{Cu-ZnO}) \quad (1)$$

$$Ag_2O + hv \rightarrow e^{-}\left(CB_{Ag_2O}\right) + h^{+}\ (VB_{Ag_2O}) \quad (2)$$

$$e^{-}\left(CB_{Ag_2O}\right) \rightarrow e^{-}(CB_{Cu-ZnO}) \quad (3)$$

$$h^{+}\ (VB_{Cu-ZnO}) \rightarrow h^{+}\ (VB_{Ag_2O}) \quad (4)$$

$$e^{-} + O_2 \rightarrow \cdot O_2^{-} \quad (5)$$

$$h^{+} + OH^{-} \rightarrow \cdot OH \quad (6)$$

$$\cdot OH + MB\ dye \rightarrow Co_2 + H_2O + Other\ byproducts \quad (7)$$

$$\cdot O_2^{-} + MB\ dye \rightarrow Co_2 + H_2O + Other\ byproducts \quad (8)$$

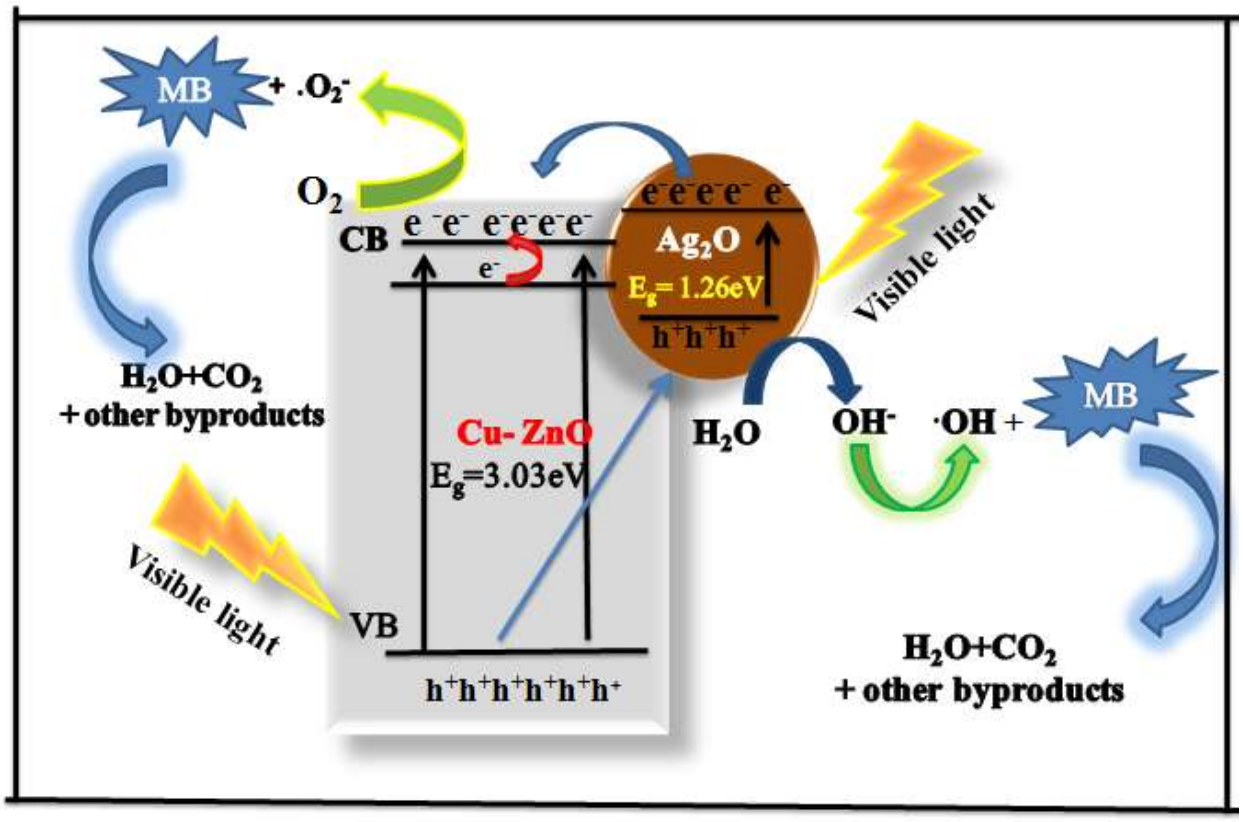

Figure 4.7. Schematic diagram for degradation mechanism of Methylene blue using CZA-10.2 catalyst under visible-light light irradiation.

Reusability test

The reusability of the CZA-10.2 composite photocatalyst was investigated under visible light irradiation with three repeated tests within 100min under visible light irradiation. As shown in Figure 4.8. The stability of CZA-10.2 was very good and it possesses high ability (78%) to degrade the Methylene blue dye after three times reused. The first possible reason we will reason out for the decrement of the photocatalytic performance of CZA-10.2 catalyst goes for the extravagant decantation during experimental regime. On the other hand, the reason behind its degradation capacity (stability) goes for reports in previous literature researches' that ,the stability of Ag_2O based catalyst is attributed to the phenomena occurred during photocatalytic reaction at which the photon-induced electrons stalk themselves to Ag^+ and form metallic Ag. Then those metallic Ag will cover the Ag_2O surfaces; which prevents the reduction of Ag_2O in to other forms. Therefore, the CZA-10.2 composite catalyst is such promising photocatalyst, so that it can be useful for real world industrial wastewater treatment application.

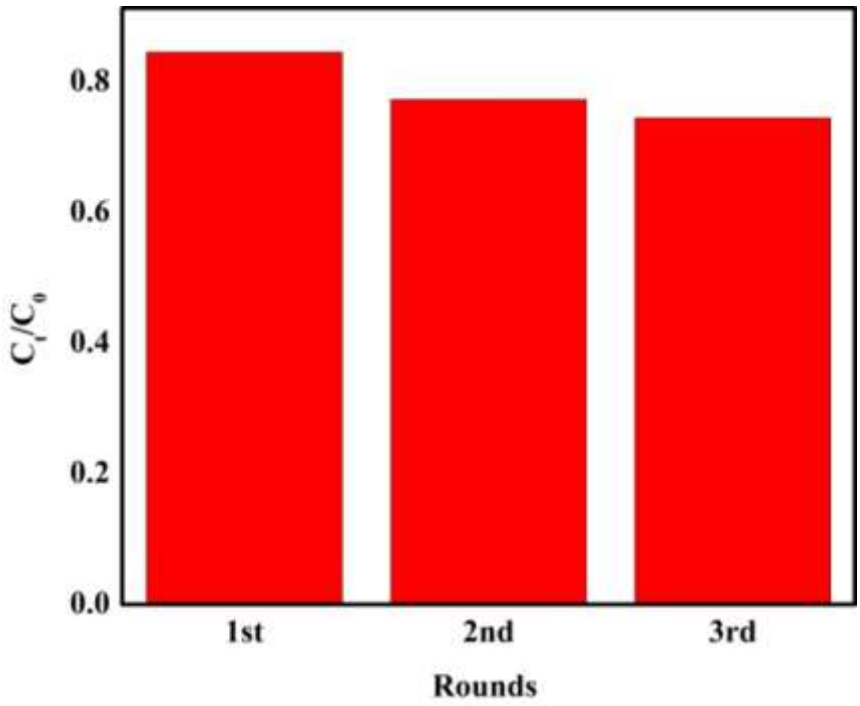

Figure 4.8. Reusability test for photocatalytic degradation of Methylene blue under Visible light irradiation

Effect of calcination temperature on the photocatalytic performance of CZA-10.2 catalyst

It is accepted that the photocatalytic performance of cellulose templated metal oxide heterostructures are mainly depends on the calcination temperature at which the cellulose will be burned out and removed from the synthesized metal oxide heterostructure [3] Eventhough, the calcinations temperature of as-synthesized CZ-2 catalyst was illustrated to be in the range of 430^0C -500^0C from the thermal analysis result, the FTIR analysis of CZ-2 after calcinations at 500^0C shows additional carbon related peak, which is attributed to stretching bond of cellulose; This indicates the incomplete removal of cellulose. Therefore, we studied the calcinations temperature effect on the catalytic activity of CZA-10.2. To study this behavior, the photocatalytic degradation efficiency of CZA-10.2 catalyst with different calcination temperatures, such as 500^0c, 600^0c and 700^0c, respectively was tested towards MB degradation under visible light illumination. Accordingly, CZA-10.2 catalyst with 600^0c calcinations temperature showed higher photocatalytic performance over the degradation of MB. This higher efficiency of photodegradation may be attributed to the complete removal of cellulose and achievement of the expected porosity, which may give more active sites for the main photocatalytic reactions, Shidpour et al, reported similar results [199]. The photocatalytic performance of CZA catalysts with calcinations temperatures of 500^0c and 700^0c were found to be decreased. This is attributed due to the fact that most of carbon based polymeric structures may not be totally removed at relative low temperatures, i.e., below 500^0c [200]. On the other hand, at relatively high temperatures (i.e., above 700^0c), the porosity attained by removing the cellulose at around 600^0c will be narrowed when it is treated with extreme high temperature as they are ceramics [201]. Therefore, the photocatalytic performance of CZA-10.2 catalyst at 700^0c was also found to be decreased; this is because of the decrement of active sites owing to diminished surface area [5]. Accordingly, the photocatalytic performance of CZA-10.2 calcined at 600^0c showed a relatively better photocatalytic performance than others, because of the complete removal of cellulose and achieving of the expected porosity.

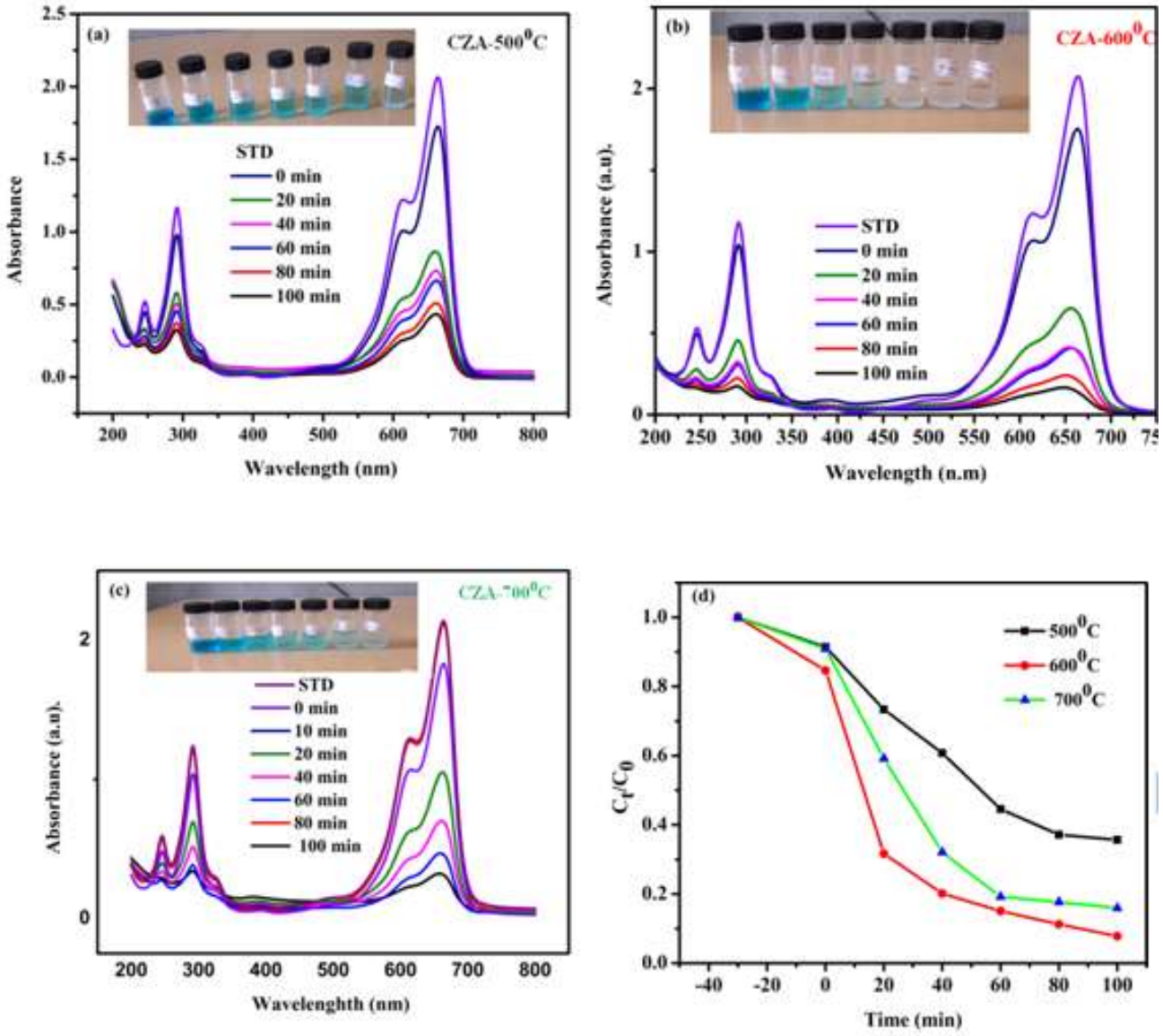

Figure 4.9. UV–vis absorption spectra for CZA-10.2 catalyst calcined at different temperatures , such as, (a) 500^{0}C and (b) 600^{0}C and (C) 700^{0}C

CHAPTER FIVE

5.Conclusions and Recommendations

5.1. Conclusion

The $Zn_{1-x}Cu_xO_x$, (x= 0.01, 0.02, 0.03 and 0.04) particles and $Zn_{0.98}Cu_{0.02}O/Ag_2O$ composites were synthesized using cellulose aided green co-prerciptation method. The cellulose was extracted from unwanted water hyacinth (Eichhornia crassipes) plant as a template. The synthesized catalysts were characterized using XRD, SEM, UV-Vis spectroscopy, FTIR, and DTG. The photocatalaytic activities of as-synthesized catalysts were pereformed through two consecutive optimizations over the degradation of methylene blue under visible light irrdation. The first optimization was performed on $Zn_{1-x}Cu_xO_x$, (x= 0.01, 0.02, 0.03 and 0.04) and $Zn_{0.98}Cu_{0.02}O$ catalyst abbreviated as CZ-2 was the optimum catalyst with 82% of degradation capacity over methylene blue dye within 100 min of visible light irradiation. Consequently, $Zn_{0.98}Cu_{0.02}O/Ag_2O$ composites with different amounts of Ag_2O (6.8%, 13.6%, 10.2% and 20.4%) were optimized over degradation of methylene blue. Among them the CZA-10.2 composite catalyst prepared with 10.2 % of Ag_2O showed the highest degradation efficiency (92%) over methylene blue dye within 100 min of visible light-irradiation. Therefore, CZ-10.2 composite catalyst was founded to be the best catalyst of this work. Furthermore, we also studied the effect of calcinations temperature and pH values on the photocatalytic activity of CZA-10.2 catalyst, as a result CZA-10.2 calcined at 600^0C showed best degradation performance (92%) and CZA-10.2 at pH=11.5 showed best performance (100% in 40 min) in basic medium.

Finally, we observed that doping of Cu on ZnO improve the visible light absorption capacity of ZnO (Figure 4.7) and Coupling of Cu-ZnO with Ag_2O semiconductor enhances electron–hole separation and enhances its visible light absorption trough shifting its optical band gap from 3.14eV-2.85eV [132]. Therefore, the combination of p-type Ag_2O and n-type Cu-doped ZnO semiconductors are promising real world applicable catalysts. On the other hand, on this work, we used unwanted plant water hyacinth for the extraction of cellulose. Currently, Our country's hot issue regarding water resources belongs to removing Water hyacinth. Accordingly, this work will play a significant role through utilization of Water hyacinth for useful purpose.

5.2. Recommendations

- In the photo degradation of organic pollutants, the availability of active specious such as, holes (h^{+}), hydroxyl radicals (•OH) and superoxide anion radicals ($\bullet O_2^-$) are very crucial and play a significant role in the photocatalytic reaction [202]. Therefore, trapping experiments are essential for identifying the role of active radicals in the photocatalysis reaction. Unfortunately we couldn't perform that experiment because of unavailability of trapping agents. Therefore, we recommend this for the next researchers to perform trapping experiment and get full information about their catalyst during the photocatalysis reaction.
- Furthermore, we have tried to characterize the as-synthesized catalysts with instruments which are available in Ethiopia. However further characterizations like, TEM for more detailed morphological analysis and determining the particle size of the samples, XPS for detailed elemental analysis with their oxidation number, Mott-schottcky analyze for assuring the formation of p-n hetrojunction, PL analysis for studying the electron-hole recombination rate of each sample and BET for determination of specific surface area of the synthesized samples, were necessary. Those instruments are not available in our country, Ethiopia. Therefore we send the samples to Taiwan Science and Technology University for further characterizations; however we couldn't get the results because of current COVID-19 situation of the world. Hence, we recommend the upcoming researchers on this area to fulfill those characterizations for further confirmation of their work.

Reference

1. Andreozzi, R., et al., *Advanced oxidation processes (AOP) for water purification and recovery.* Catalysis today, 1999. **53**(1): p. 51-59.
2. Serpone, N. and A.V. Emeline, *Semiconductor Photocatalysis - Past, Present, and Future Outlook.* J Phys Chem Lett, 2012. **3**(5): p. 673-7.
3. Lin, Z., Y. Lu, and J. Huang, *A hierarchical Ag2O-nanoparticle/TiO2-nanotube composite derived from natural cellulose substance with enhanced photocatalytic performance.* Cellulose, 2019. **26**(11): p. 6683-6700.
4. Kale, G., et al., *Paper templated synthesis of nanostructured Cu–ZnO and its enhanced photocatalytic activity under sunlight.* Journal of Materials Science: Materials in Electronics, 2019. **30**(7): p. 7031-7042.
5. Saravanan, R., F. Gracia, and A. Stephen, *Basic Principles, Mechanism, and Challenges of Photocatalysis.* 2017: p. 19-40.
6. You, J., et al., *A review of visible light-active photocatalysts for water disinfection: Features and prospects.* Chemical Engineering Journal, 2019. **373**: p. 624-641.
7. Bora, T. and J. Dutta, *Applications of nanotechnology in wastewater treatment--a review.* J Nanosci Nanotechnol, 2014. **14**(1): p. 613-26.
8. Amin, M.T., A.A. Alazba, and U. Manzoor, *A Review of Removal of Pollutants from Water/Wastewater Using Different Types of Nanomaterials.* Advances in Materials Science and Engineering, 2014. **2014**: p. 1-24.
9. Liu, L., et al., *Removal of Cryptosporidium surrogates in drinking water direct filtration.* Colloids Surf B Biointerfaces, 2019. **181**: p. 499-505.
10. Ma, J., et al., *Drinking water treatment by stepwise flocculation using polysilicate aluminum magnesium and cationic polyacrylamide.* Journal of Environmental Chemical Engineering, 2019. **7**(3): p. 103049.
11. Riaz, R., et al., *Activated charcoal and reduced graphene sheets composite structure for highly electro-catalytically active counter electrode material and water treatment.* International Journal of Hydrogen Energy, 2019.
12. Wang, L., et al., *17α-Ethinylestradiol removal from water by magnetic ion exchange resin.* Chinese Journal of Chemical Engineering, 2018. **26**(4): p. 864-869.

13. Bora, L.V. and R.K. Mewada, *Visible/solar light active photocatalysts for organic effluent treatment: Fundamentals, mechanisms and parametric review.* Renewable and Sustainable Energy Reviews, 2017. **76**: p. 1393-1421.
14. Ding, W., et al., *Bovine serum albumin assisted synthesis of Ag/Ag2O/ZnO photocatalyst with enhanced photocatalytic activity under visible light.* Colloids and Surfaces A: Physicochemical and Engineering Aspects, 2019. **568**: p. 131-140.
15. Qu, X., P.J. Alvarez, and Q. Li, *Applications of nanotechnology in water and wastewater treatment.* Water Res, 2013. **47**(12): p. 3931-46.
16. Babuponnusami, A. and K. Muthukumar, *A review on Fenton and improvements to the Fenton process for wastewater treatment.* Journal of Environmental Chemical Engineering, 2014. **2**(1): p. 557-572.
17. Gogate, P.R. and A.B. Pandit, *A review of imperative technologies for wastewater treatment I: oxidation technologies at ambient conditions.* Advances in Environmental Research, 2004. **8**(3-4): p. 501-551.
18. Gogate, P.R. and A.B. Pandit, *A review of imperative technologies for wastewater treatment II: hybrid methods.* Advances in environmental research, 2004. **8**(3-4): p. 553-597.
19. Fujishima, A. and K. Honda, *Electrochemical photolysis of water at a semiconductor electrode.* nature, 1972. **238**(5358): p. 37-38.
20. Hlongwane, G.N., et al., *Simultaneous removal of pollutants from water using nanoparticles: A shift from single pollutant control to multiple pollutant control.* Sci Total Environ, 2019. **656**: p. 808-833.
21. Tang, G., A. Abas, and S. Wang, *Photocatalytic Degradation and Hydrogen Production of TiO2/Carbon Fiber Composite Using Bast as a Carbon Fiber Source.* International Journal of Photoenergy, 2018. **2018**: p. 1-8.
22. Ganguly, P., et al., *Antimicrobial activity of photocatalysts: Fundamentals, mechanisms, kinetics and recent advances.* Applied Catalysis B: Environmental, 2018. **225**: p. 51-75.
23. Rajeshwar, K., et al., *Heterogeneous photocatalytic treatment of organic dyes in air and aqueous media.* Journal of Photochemistry and Photobiology C: Photochemistry Reviews, 2008. **9**(4): p. 171-192.

24. Jamil, T.S., et al., *Homogeneous photocatalytic processes for degradation of some endocrine disturbing chemicals under UV irradiation.* Journal of Water Process Engineering, 2017. **18**: p. 159-168.
25. Thao, N.P., et al., *Role of ethylene and its cross talk with other signaling molecules in plant responses to heavy metal stress.* Plant physiology, 2015. **169**(1): p. 73-84.
26. Nakata, K. and A. Fujishima, *TiO2 photocatalysis: Design and applications.* Journal of photochemistry and photobiology C: Photochemistry Reviews, 2012. **13**(3): p. 169-189.
27. Hatamie, A., et al., *Zinc oxide nanostructure-modified textile and its application to biosensing, photocatalysis, and as antibacterial material.* Langmuir, 2015. **31**(39): p. 10913-10921.
28. Rehman, S., et al., *Strategies of making TiO2 and ZnO visible light active.* Journal of hazardous materials, 2009. **170**(2-3): p. 560-569.
29. Rajeshwar, K., et al., *Heterogeneous photocatalytic treatment of organic dyes in air and aqueous media.* Journal of photochemistry and photobiology C: photochemistry reviews, 2008. **9**(4): p. 171-192.
30. Saravanan, S., et al., *Preparation, characterization and antimicrobial activity of a bio-composite scaffold containing chitosan/nano-hydroxyapatite/nano-silver for bone tissue engineering.* International journal of biological macromolecules, 2011. **49**(2): p. 188-193.
31. Wang, Y., et al., *Sm–Co hard magnetic nanoparticles prepared by surfactant-assisted ball milling.* Nanotechnology, 2007. **18**(46): p. 465701.
32. Reza, K.M., A. Kurny, and F. Gulshan, *Parameters affecting the photocatalytic degradation of dyes using TiO 2: a review.* Applied Water Science, 2017. **7**(4): p. 1569-1578.
33. Gnanasekaran, L., R. Hemamalini, and K. Ravichandran, *Synthesis and characterization of TiO2 quantum dots for photocatalytic application.* Journal of Saudi Chemical Society, 2015. **19**(5): p. 589-594.
34. Choquette-Labbé, M., et al., *Photocatalytic degradation of phenol and phenol derivatives using a nano-TiO2 catalyst: Integrating quantitative and qualitative factors using response surface methodology.* Water, 2014. **6**(6): p. 1785-1806.

35. Wang, W.W., Y.J. Zhu, and L.X. Yang, *ZnO–SnO2 hollow spheres and hierarchical nanosheets: hydrothermal preparation, formation mechanism, and photocatalytic properties.* Advanced Functional Materials, 2007. **17**(1): p. 59-64.
36. Jiang, T., et al., *Carbon nanotubes/TiO2 nanotubes composite photocatalysts for efficient degradation of methyl orange dye.* Particuology, 2013. **11**(6): p. 737-742.
37. Saravanan, R., et al., *Synthesis, characterization and photocatalytic activity of novel Hg doped ZnO nanorods prepared by thermal decomposition method.* Journal of Molecular Liquids, 2013. **178**: p. 88-93.
38. Cernuto, G., et al., *Size and shape dependence of the photocatalytic activity of TiO2 nanocrystals: a total scattering Debye function study.* Journal of the American Chemical Society, 2011. **133**(9): p. 3114-3119.
39. Omar, F.S., et al., *Microwave synthesis of zinc oxide/reduced graphene oxide hybrid for adsorption-photocatalysis application.* International Journal of Photoenergy, 2014. **2014**.
40. Saravanan, R., F. Gracia, and A. Stephen, *Basic principles, mechanism, and challenges of photocatalysis*, in *Nanocomposites for visible light-induced photocatalysis*. 2017, Springer. p. 19-40.
41. Malato, S., et al., *Decontamination and disinfection of water by solar photocatalysis: recent overview and trends.* Catalysis today, 2009. **147**(1): p. 1-59.
42. Mohapatra, D.P., et al., *Photocatalytic degradation of carbamazepine in wastewater by using a new class of whey-stabilized nanocrystalline TiO2 and ZnO.* Science of the total environment, 2014. **485**: p. 263-269.
43. Wong, C.L., Y.N. Tan, and A.R. Mohamed, *A review on the formation of titania nanotube photocatalysts by hydrothermal treatment.* Journal of Environmental Management, 2011. **92**(7): p. 1669-1680.
44. Chatterjee, D. and S. Dasgupta, *Visible light induced photocatalytic degradation of organic pollutants.* Journal of Photochemistry and Photobiology C: Photochemistry Reviews, 2005. **6**(2-3): p. 186-205.
45. Kazeminezhad, I. and A. Sadollahkhani, *Influence of pH on the photocatalytic activity of ZnO nanoparticles.* Journal of Materials Science: Materials in Electronics, 2016. **27**(5): p. 4206-4215.

46. Castillo-Ledezma, J., et al., *Effect of pH, solar irradiation, and semiconductor concentration on the photocatalytic disinfection of Escherichia coli in water using nitrogen-doped TiO 2.* European Food Research and Technology, 2011. **233**(5): p. 825.
47. Sakthivel, S., et al., *Solar photocatalytic degradation of azo dye: comparison of photocatalytic efficiency of ZnO and TiO2.* Solar energy materials and solar cells, 2003. **77**(1): p. 65-82.
48. Spasiano, D., et al., *Solar photocatalysis: Materials, reactors, some commercial, and pre-industrialized applications. A comprehensive approach.* Applied Catalysis B: Environmental, 2015. **170**: p. 90-123.
49. Qi, K. and J. Yu, *Chapter 8 - Modification of ZnO-based photocatalysts for enhanced photocatalytic activity*, in *Interface Science and Technology*, J. Yu, M. Jaroniec, and C. Jiang, Editors. 2020, Elsevier. p. 265-284.
50. Li, J. and N. Wu, *Semiconductor-based photocatalysts and photoelectrochemical cells for solar fuel generation: a review.* Catalysis Science & Technology, 2015. **5**(3): p. 1360-1384.
51. Hisatomi, T., J. Kubota, and K. Domen, *Recent advances in semiconductors for photocatalytic and photoelectrochemical water splitting.* Chemical Society Reviews, 2014. **43**(22): p. 7520-7535.
52. Hoffmann, M.R., et al., *Environmental applications of semiconductor photocatalysis.* Chemical reviews, 1995. **95**(1): p. 69-96.
53. Akerdi, A.G. and S.H. Bahrami, *Application of heterogeneous nano-semiconductors for photocatalytic advanced oxidation of organic compounds: A review.* Journal of Environmental Chemical Engineering, 2019. **7**(5): p. 103283.
54. Wang, H., et al., *Semiconductor heterojunction photocatalysts: design, construction, and photocatalytic performances.* Chemical Society Reviews, 2014. **43**(15): p. 5234-5244.
55. Li, D., et al., *A versatile bio-based material for efficiently removing toxic dyes, heavy metal ions and emulsified oil droplets from water simultaneously.* Bioresource technology, 2017. **245**: p. 649-655.
56. Tee, S.Y., C.P. Teng, and E. Ye, *Metal nanostructures for non-enzymatic glucose sensing.* Materials Science and Engineering: C, 2017. **70**: p. 1018-1030.

57. Alamelu, K. and B.M. Jaffar Ali, *TiO2-Pt composite photocatalyst for photodegradation and chemical reduction of recalcitrant organic pollutants.* Journal of Environmental Chemical Engineering, 2018. **6**(5): p. 5720-5731.
58. Zheng, B., et al., *Energy - transfer modulation for enhanced photocatalytic activity of near - infrared upconversion photocatalyst.* Journal of the American Ceramic Society, 2015. **98**(1): p. 136-140.
59. A. Escobar Barrios, V., et al., *Modified Metallic Oxides for Efficient Photocatalysis.* 2019.
60. Umezawa, N. and J. Ye, *Role of complex defects in photocatalytic activities of nitrogen-doped anatase TiO 2.* Physical Chemistry Chemical Physics, 2012. **14**(17): p. 5924-5934.
61. Liu, S.X., et al., *Gliding arc plasma synthesis of visible - light active C - doped titania photocatalysts.* Plasma Processes and Polymers, 2015. **12**(5): p. 422-430.
62. Li, M., et al., *Enhanced visible light responsive photocatalytic activity of TiO 2-based nanocrystallites: impact of doping sequence.* RSC Advances, 2015. **5**(10): p. 7363-7369.
63. Song, K., X. Han, and G. Shao, *Electronic properties of rutile TiO2 doped with 4d transition metals: First-principles study.* Journal of Alloys and Compounds, 2013. **551**: p. 118-124.
64. Yu, X., et al., *The influence of defects on Mo - doped TiO2 by first - principles studies.* ChemPhysChem, 2012. **13**(6): p. 1514-1521.
65. Liu, L. and X. Chen, *Titanium dioxide nanomaterials: self-structural modifications.* Chemical reviews, 2014. **114**(19): p. 9890-9918.
66. Xing, M., X. Li, and J. Zhang, *Synergistic effect on the visible light activity of Ti 3+ doped TiO 2 nanorods/boron doped graphene composite.* Scientific reports, 2014. **4**: p. 5493.
67. De Angelis, F., et al., *Influence of the sensitizer adsorption mode on the open-circuit potential of dye-sensitized solar cells.* Nano letters, 2007. **7**(10): p. 3189-3195.
68. Huang, F., A. Yan, and H. Zhao, *Influences of doping on photocatalytic properties of TiO2 photocatalyst.* Semiconductor Photocatalysis—Materials, Mechanisms and Applications; Cao, W., Ed, 2016: p. 31-80.
69. Štengl, V.c., et al., *Photocatalytic activity of boron-modified titania under UV and visible-light illumination.* ACS applied materials & interfaces, 2010. **2**(2): p. 575-580.

70. Patel, N., et al., *Experimental and theoretical investigations on the activity and stability of substitutional and interstitial boron in TiO2 photocatalyst.* The Journal of Physical Chemistry C, 2015. **119**(32): p. 18581-18590.

71. Bolokang, A., et al., *Morphology and structural development of reduced anatase-TiO2 by pure Ti powder upon annealing and nitridation: Synthesis of TiOx and TiOxNy powders.* Materials Characterization, 2015. **100**: p. 41-49.

72. Lynch, J., et al., *Substitutional or interstitial site-selective nitrogen doping in TiO2 nanostructures.* The Journal of Physical Chemistry C, 2015. **119**(13): p. 7443-7452.

73. El-Sheikh, S.M., et al., *High performance sulfur, nitrogen and carbon doped mesoporous anatase–brookite TiO2 photocatalyst for the removal of microcystin-LR under visible light irradiation.* Journal of hazardous materials, 2014. **280**: p. 723-733.

74. Yu, J., et al., *Fabrication and enhanced visible-light photocatalytic activity of carbon self-doped TiO 2 sheets with exposed {001} facets.* Journal of Materials Chemistry, 2011. **21**(4): p. 1049-1057.

75. Li, Z., et al., *Synthesis and characterization of sulfated TiO2 nanorods and ZrO2/TiO2 nanocomposites for the esterification of biobased organic acid.* ACS applied materials & interfaces, 2012. **4**(9): p. 4499-4505.

76. Tipayarom, D., K. Wantala, and N. Grisdanurak, *Optimization of alachlor degradation on S-doped TiO (2) by sonophotocatalytic activity under visible light.* 2011.

77. Senna, M., et al., *Introduction of oxygen vacancies and fluorine into TiO2 nanoparticles by co-milling with PTFE.* Journal of Solid State Chemistry, 2012. **187**: p. 51-57.

78. Qiao, Z.a., et al., *A topotactic synthetic methodology for highly fluorine - doped mesoporous metal oxides.* Angewandte Chemie, 2012. **124**(12): p. 2942-2947.

79. Ji, P.L., et al., *Characterization and photocatalytic properties of silver and silver chloride doped TiO2 hollow nanoparticles.* Chinese Chemical Letters, 2012. **23**(12): p. 1399-1402.

80. Xu, H., et al., *Hierarchical chlorine-doped rutile TiO2 spherical clusters of nanorods: Large-scale synthesis and high photocatalytic activity.* Journal of Solid State Chemistry, 2008. **181**(9): p. 2516-2522.

81. Nagaveni, K., et al., *Synthesis and structure of nanocrystalline TiO2 with lower band gap showing high photocatalytic activity.* Langmuir, 2004. **20**(7): p. 2900-2907.

82. Chen, L.-C., et al., *Characterization and photoreactivity of N-, S-, and C-doped ZnO under UV and visible light illumination.* Journal of Photochemistry and Photobiology A: Chemistry, 2008. **199**(2-3): p. 170-178.

83. Yu, W., J. Zhang, and T. Peng, *New insight into the enhanced photocatalytic activity of N-, C- and S-doped ZnO photocatalysts.* Applied Catalysis B: Environmental, 2016. **181**: p. 220-227.

84. Samadi, M., et al., *Recent progress on doped ZnO nanostructures for visible-light photocatalysis.* Thin Solid Films, 2016. **605**: p. 2-19.

85. Shen, Y., et al., *Tungsten and nitrogen co-doped TiO2 nano-powders with strong visible light response.* Applied Catalysis B: Environmental, 2008. **83**(3-4): p. 177-185.

86. Liu, C., et al., *Characterization and activity of visible-light-driven TiO2 photocatalyst codoped with nitrogen and cerium.* Journal of Solid State Chemistry, 2008. **181**(4): p. 913-919.

87. Kim, S.W., et al., *Synthesis, Characterization, and Application of Zr, S Co-doped TiO~ 2 as Visible-light Active Photocatalyst.* Bulletin-Korean Chemical Society, 2008. **29**(6): p. 1217.

88. Morikawa, T., Y. Irokawa, and T. Ohwaki, *Enhanced photocatalytic activity of TiO2− xNx loaded with copper ions under visible light irradiation.* Applied Catalysis A: General, 2006. **314**(1): p. 123-127.

89. Lavanya, T., et al., *Superior photocatalytic performance of reduced graphene oxide wrapped electrospun anatase mesoporous TiO2 nanofibers.* Journal of alloys and compounds, 2014. **615**: p. 643-650.

90. Nenavathu, B.P., et al., *Synthesis, characterization and enhanced photocatalytic degradation efficiency of Se doped ZnO nanoparticles using trypan blue as a model dye.* Applied Catalysis A: General, 2013. **459**: p. 106-113.

91. Pelaez, M., et al., *A Review on the Visible Light Active Titanium Dioxide Photocatalysts for Environmental Applications.* Applied Catalysis B Environmental, 2012. **125**: p. 331-349.

92. Wu, C., et al., *Solvothermal synthesis of Cr-doped ZnO nanowires with visible light-driven photocatalytic activity.* Materials Letters, 2011. **65**(12): p. 1794-1796.

93. Wu, C., et al., *Solvothermal synthesis of Cu-doped ZnO nanowires with visible light-driven photocatalytic activity.* Materials Letters, 2012. **74**: p. 236-238.
94. Peng, Y., et al., *Fabrication of porous Cd-doped ZnO nanorods with enhanced photocatalytic activity and stability.* CrystEngComm, 2013. **15**(33): p. 6518-6525.
95. Thennarasu, G. and A. Sivasamy, *Metal ion doped semiconductor metal oxide nanosphere particles prepared by soft chemical method and its visible light photocatalytic activity in degradation of phenol.* Powder technology, 2013. **250**: p. 1-12.
96. Qi, K., et al., *Transition metal doped ZnO nanoparticles with enhanced photocatalytic and antibacterial performances: Experimental and DFT studies.* Ceramics International, 2019.
97. Kaneva, N.V., D.T. Dimitrov, and C.D. Dushkin, *Effect of nickel doping on the photocatalytic activity of ZnO thin films under UV and visible light.* Applied Surface Science, 2011. **257**(18): p. 8113-8120.
98. Saleh, R. and N.F. Djaja, *Transition-metal-doped ZnO nanoparticles: synthesis, characterization and photocatalytic activity under UV light.* Spectrochimica Acta Part A: Molecular and Biomolecular Spectroscopy, 2014. **130**: p. 581-590.
99. Zhang, Q., et al., *Atmospheric self-induction synthesis and enhanced visible light photocatalytic performance of Fe3+ doped Ag-ZnO mesocrystals.* Industrial & Engineering Chemistry Research, 2014. **53**(34): p. 13236-13246.
100. He, R., R.K. Hocking, and T. Tsuzuki, *Co-doped ZnO nanopowders: location of cobalt and reduction in photocatalytic activity.* Materials Chemistry and Physics, 2012. **132**(2-3): p. 1035-1040.
101. Yin, Q., et al., *Hierarchical nanostructures of nickel-doped zinc oxide: morphology controlled synthesis and enhanced visible-light photocatalytic activity.* Journal of alloys and compounds, 2015. **618**: p. 318-325.
102. Ullah, R. and J. Dutta, *Photocatalytic degradation of organic dyes with manganese-doped ZnO nanoparticles.* Journal of Hazardous materials, 2008. **156**(1-3): p. 194-200.
103. Chang, C.-J., T.-L. Yang, and Y.-C. Weng, *Synthesis and characterization of Cr-doped ZnO nanorod-array photocatalysts with improved activity.* Journal of Solid State Chemistry, 2014. **214**: p. 101-107.

104. Slama, R., et al., *Visible photocatalytic properties of vanadium doped zinc oxide aerogel nanopowder.* Thin Solid Films, 2011. **519**(17): p. 5792-5795.
105. Jiang, J., et al., *Insights into the synergetic effect for enhanced UV/visible-light activated photodegradation activity via Cu-ZnO photocatalyst.* Applied Surface Science, 2019. **478**: p. 1037-1045.
106. Clament Sagaya Selvam, N., J.J. Vijaya, and L.J. Kennedy, *Effects of morphology and Zr doping on structural, optical, and photocatalytic properties of ZnO nanostructures.* Industrial & engineering chemistry research, 2012. **51**(50): p. 16333-16345.
107. Kubacka, A., M. Fernández-García, and G. Colón, *Advanced Nanoarchitectures for Solar Photocatalytic Applications.* Chemical reviews, 2012. **112**: p. 1555-614.
108. Mittal, M., M. Sharma, and O.P. Pandey, *UV–Visible light induced photocatalytic studies of Cu doped ZnO nanoparticles prepared by co-precipitation method.* Solar Energy, 2014. **110**: p. 386-397.
109. Polat, İ., et al., *The influence of Cu-doping on structural, optical and photocatalytic properties of ZnO nanorods.* Materials Chemistry and Physics, 2014. **148**(3): p. 528-532.
110. Kuriakose, S., B. Satpati, and S. Mohapatra, *Enhanced photocatalytic activity of Co doped ZnO nanodisks and nanorods prepared by a facile wet chemical method.* Physical Chemistry Chemical Physics, 2014. **16**(25): p. 12741-12749.
111. Alam, U., et al., *Highly efficient Y and V co-doped ZnO photocatalyst with enhanced dye sensitized visible light photocatalytic activity.* Catalysis Today, 2017. **284**: p. 169-178.
112. Achouri, F., et al., *Porous Mn-doped ZnO nanoparticles for enhanced solar and visible light photocatalysis.* Materials & Design, 2016. **101**: p. 309-316.
113. Pirzada, B.M., et al., *Efficient visible-light-driven Photocatalytic activity and enhanced charge transfer properties over Mo-doped WO3/TiO2 nanocomposites.* Journal of Environmental Chemical Engineering, 2018. **6**(2): p. 3204-3212.
114. Sood, S., et al., *Highly effective Fe-doped TiO2 nanoparticles photocatalysts for visible-light driven photocatalytic degradation of toxic organic compounds.* Journal of Colloid and Interface Science, 2015. **450**: p. 213-223.
115. Ali, T., et al., *Enhanced photocatalytic and antibacterial activities of Ag-doped TiO2 nanoparticles under visible light.* Materials Chemistry and Physics, 2018. **212**: p. 325-335.

116. Kuriakose, S., B. Satpati, and S. Mohapatra, *Highly efficient photocatalytic degradation of organic dyes by Cu doped ZnO nanostructures.* Physical Chemistry Chemical Physics, 2015. **17**(38): p. 25172-25181.

117. Pawar, R.C., et al., *Formation of polar surfaces in microstructured ZnO by doping with Cu and applications in photocatalysis using visible light.* Materials Chemistry and Physics, 2015. **151**: p. 167-180.

118. Vaiano, V., G. Iervolino, and L. Rizzo, *Cu-doped ZnO as efficient photocatalyst for the oxidation of arsenite to arsenate under visible light.* Applied Catalysis B: Environmental, 2018. **238**: p. 471-479.

119. Jongnavakit, P., et al., *Preparation and photocatalytic activity of Cu-doped ZnO thin films prepared by the sol–gel method.* Applied Surface Science, 2012. **258**(20): p. 8192-8198.

120. Mittal, M., M. Sharma, and O. Pandey, *UV–Visible light induced photocatalytic studies of Cu doped ZnO nanoparticles prepared by co-precipitation method.* Solar Energy, 2014. **110**: p. 386–397.

121. Mohan, R., K. Krishnamoorthy, and S.-J. Kim, *Enhanced photocatalytic activity of Cu-doped ZnO nanorods.* Solid State Communications, 2012. **152**(5): p. 375-380.

122. Wang, S., et al., *Recent Progress on Visible Light Responsive Heterojunctions for Photocatalytic Applications.* Journal of Materials Science & Technology, 2017. **33**(1): p. 1-22.

123. Qi, K., et al., *Review on the improvement of the photocatalytic and antibacterial activities of ZnO.* Journal of Alloys and Compounds, 2017. **727**: p. 792-820.

124. Wang, X., et al., *Stable photocatalytic hydrogen evolution from water over ZnO–CdS core–shell nanorods.* International Journal of Hydrogen Energy, 2010. **35**(15): p. 8199-8205.

125. Cho, S., et al., *Three-Dimensional Type II ZnO/ZnSe Heterostructures and Their Visible Light Photocatalytic Activities.* Langmuir, 2011. **27**(16): p. 10243-10250.

126. Wang, Z., et al., *Highly Photocatalytic ZnO/In2O3 Heteronanostructures Synthesized by a Coprecipitation Method.* The Journal of Physical Chemistry C, 2009. **113**(11): p. 4612-4617.

127. Chabri, S., et al., *Mesoporous CuO–ZnO p–n heterojunction based nanocomposites with high specific surface area for enhanced photocatalysis and electrochemical sensing.* Catalysis Science & Technology, 2016. **6**(9): p. 3238-3252.
128. Wang, J., et al., *Hybrid Ag2O/ZnO Heterostructures.* Journal of Nanomaterials, 2013. **2013**: p. 1-5.
129. Wang, X., et al., *Ag2O as a new visible-light photocatalyst: self-stability and high photocatalytic activity.* Chemistry, 2011. **17**(28): p. 7777-80.
130. Wang, X., et al., *Ag2O as a new visible - light photocatalyst: self - stability and high photocatalytic activity.* Chemistry–A European Journal, 2011. **17**(28): p. 7777-7780.
131. Paul, K.K., R. Ghosh, and P.K. Giri, *Mechanism of strong visible light photocatalysis by Ag2O-nanoparticle-decorated monoclinic TiO2(B) porous nanorods.* Nanotechnology, 2016. **27**(31): p. 315703.
132. Kadam, A., et al., *Template free synthesis of ZnO/Ag2O nanocomposites as a highly efficient visible active photocatalyst for detoxification of Methyl Orange.* Journal of Photochemistry and Photobiology B Biology, 2015. **154**: p. 24-33.
133. Cui, L., J. Wu, and H. Ju, *Electrochemical sensing of heavy metal ions with inorganic, organic and bio-materials.* Biosensors and Bioelectronics, 2015. **63**: p. 276-286.
134. Tian, W., et al., *Bio-inspired beehive-like hierarchical nanoporous carbon derived from bamboo-based industrial by-product as a high performance supercapacitor electrode material.* Journal of Materials Chemistry A, 2015. **3**(10): p. 5656-5664.
135. Wang, Z.J., et al., *Bandgap Engineering of Conjugated Nanoporous Poly - benzobisthiadiazoles via Copolymerization for Enhanced Photocatalytic 1, 2, 3, 4 - Tetrahydroquinoline Synthesis under Visible Light.* Advanced Synthesis & Catalysis, 2016. **358**(16): p. 2576-2582.
136. Colmenares, J.C. and E. Kuna, *Photoactive Hybrid Catalysts Based on Natural and Synthetic Polymers: A Comparative Overview.* Molecules, 2017. **22**(5).
137. Sabar, S., M. Nawi, and W. Ngah, *Photocatalytic removal of Reactive Red 4 dye by immobilised layer-by-layer TiO2/cross-linked chitosan derivatives system.* Desalination and Water Treatment, 2016. **57**(13): p. 5851-5857.

138. Hamdi, A., S. Boufi, and S. Bouattour, *Phthalocyanine/chitosan-TiO2 photocatalysts: characterization and photocatalytic activity.* Applied Surface Science, 2015. **339**: p. 128-136.

139. Benabid, F.Z. and F. Zouai, *Natural polymers: Cellulose, chitin, chitosan, gelatin, starch, carrageenan, xylan and dextran.* Algerian Journal of Natural Products, 2016. **4**(3): p. 348-357.

140. Fu, S., P. Song, and X. Liu, *Thermal and flame retardancy properties of thermoplastics/natural fiber biocomposites*, in *Advanced High Strength Natural Fibre Composites in Construction*. 2017, Elsevier. p. 479-508.

141. Li, H., S. Fu, and L. Peng, *Surface modification of cellulose fibers by layer-by-layer self-assembly of lignosulfonates and TiO 2 nanoparticles: Effect on photocatalytic abilities and paper properties.* Fibers and Polymers, 2013. **14**(11): p. 1794-1802.

142. Zeng, J., et al., *TiO2 immobilized in cellulose matrix for photocatalytic degradation of phenol under weak UV light irradiation.* The Journal of Physical Chemistry C, 2010. **114**(17): p. 7806-7811.

143. Ten, E. and W. Vermerris, *Functionalized polymers from lignocellulosic biomass: State of the art.* Polymers, 2013. **5**(2): p. 600-642.

144. Chen, X., et al., *Synthesis and photocatalytic activity of mesoporous TiO2 nanoparticle using biological renewable resource of un-modified lignin as a template.* Microporous and Mesoporous Materials, 2016. **223**: p. 145-151.

145. Kansal, S., M. Singh, and D. Sud, *Studies on TiO2/ZnO photocatalysed degradation of lignin.* Journal of Hazardous materials, 2008. **153**(1-2): p. 412-417.

146. Pandey, K.K., *A note on the influence of extractives on the photo-discoloration and photo-degradation of wood.* Polymer degradation and stability, 2005. **87**(2): p. 375-379.

147. Chen, X., et al., *Direct conversion of chitin into a N-containing furan derivative.* Green Chemistry, 2014. **16**(4): p. 2204-2212.

148. Tang, H., W. Zhou, and L. Zhang, *Adsorption isotherms and kinetics studies of malachite green on chitin hydrogels.* Journal of hazardous materials, 2012. **209**: p. 218-225.

149. Kamal, T., et al., *Dye adsorption and bactericidal properties of TiO2/chitosan coating layer.* Carbohydrate polymers, 2016. **148**: p. 153-160.

150. Xiao, G., H. Su, and T. Tan, *Synthesis of core–shell bioaffinity chitosan–TiO2 composite and its environmental applications.* Journal of hazardous materials, 2015. **283**: p. 888-896.

151. Colmenares, J.C., R.S. Varma, and P. Lisowski, *Sustainable hybrid photocatalysts: titania immobilized on carbon materials derived from renewable and biodegradable resources.* Green chemistry, 2016. **18**(21): p. 5736-5750.

152. Haldorai, Y. and J.J. Shim, *Novel chitosan- TiO2 nanohybrid: Preparation, characterization, antibacterial, and photocatalytic properties.* Polymer Composites, 2014. **35**(2): p. 327-333.

153. Horvath, A.L., *Solubility of structurally complicated materials: II. Bone.* Journal of physical and chemical reference data, 2006. **35**(4): p. 1653-1668.

154. Lin, Z., Y. Lu, and J. Huang, *A hierarchical Ag 2 O-nanoparticle/TiO 2-nanotube composite derived from natural cellulose substance with enhanced photocatalytic performance.* Cellulose, 2019. **26**(11): p. 6683-6700.

155. Liu, Y., et al., *Optimized synthesis of FeS nanoparticles with a high Cr (VI) removal capability.* Journal of Nanomaterials, 2016. **2016**: p. 48.

156. Lu, Y., et al., *Fabrication, characterization and photocatalytic properties of millimeter-long TiO2 fiber with nanostructures using cellulose fiber as a template.* Journal of Alloys and Compounds, 2013. **577**: p. 569-574.

157. Zhou, Z., et al., *Electrospun cellulose acetate supported Ag@ AgCl composites with facet-dependent photocatalytic properties on degradation of organic dyes under visible-light irradiation.* Carbohydrate polymers, 2016. **136**: p. 322-328.

158. Richardson, J., et al., *Innovation in Layer-by-Layer Assembly.* Chemical Reviews, 2016. **116**.

159. Al-Mobarak, T., *Material Properties of Acetylated Jute-Mat Composites*. 2010.

160. Yu, D.-H., et al., *Synthesis of natural cellulose-templated TiO2/Ag nanosponge composites and photocatalytic properties.* ACS applied materials & interfaces, 2012. **4**(5): p. 2781-2787.

161. Mohamed, R., et al. *Swelling and tensile properties of starch glycerol system with various crosslinking agents*. in *IOP Conf. Ser.: Mater. Sci. Eng*. 2017.

162. Mohamed, W.Z.W., et al., *Effects of fiber size and fiber content on mechanical and physical properties of Mengkuang reinforced thermoplastic natural rubber composites.* BioResources, 2018. **13**(2): p. 2945-2959.

163. Ren, F., et al., *Facile preparation of 3D regenerated cellulose/graphene oxide composite aerogel with high-efficiency adsorption towards methylene blue.* Journal of colloid and interface science, 2018. **532**: p. 58-67.

164. Klemm, D. and D. Schumann, *U. 11. Udhardt and S. Marsch.* Prog. Polym. Sci, 2001. **26**: p. 1561-1603.

165. Barud, H.S., et al., *Antimicrobial bacterial cellulose-silver nanoparticles composite membranes.* Journal of Nanomaterials, 2011. **2011**.

166. Su, W., et al., *The Resource Utilization of Water Hyacinth (Eichhornia crassipes [Mart.] Solms) and Its Challenges.* Resources, 2018. **7**(3): p. 46.

167. Asrofi, M., et al., *XRD and FTIR Studies of Nanocrystalline Cellulose from Water Hyacinth (Eichornia crassipes) Fiber.* Journal of Metastable and Nanocrystalline Materials, 2017. **29**: p. 9-16.

168. Malik, A., *Environmental challenge vis a vis opportunity: the case of water hyacinth.* Environment international, 2007. **33**(1): p. 122-138.

169. Abdel-Fattah, A.F. and M.A. Abdel-Naby, *Pretreatment and enzymic saccharification of water hyacinth cellulose.* Carbohydrate polymers, 2012. **87**(3): p. 2109-2113.

170. Khan, S.A., et al., *Green synthesis of ZnO and Cu-doped ZnO nanoparticles from leaf extracts of Abutilon indicum, Clerodendrum infortunatum, Clerodendrum inerme and investigation of their biological and photocatalytic activities.* Mater Sci Eng C Mater Biol Appl, 2018. **82**: p. 46-59.

171. Perillo, P.M. and M.N. Atia, *Solar-assisted photodegradation of methyl orange using Cu-doped ZnO nanorods.* Materials Today Communications, 2018. **17**: p. 252-258.

172. Meshram, S.P., et al., *Cu doped ZnO microballs as effective sunlight driven photocatalyst.* Ceramics International, 2016. **42**(6): p. 7482-7489.

173. Babu, B., et al., *Room temperature ferromagnetism and optical properties of Cu2+ doped ZnO nanopowder by ultrasound assisted solid state reaction technique.* Journal of magnetism and magnetic materials, 2014. **355**: p. 76-80.

174. Allred, A., *Electronegativity values from thermochemical data.* Journal of inorganic and nuclear chemistry, 1961. **17**(3-4): p. 215-221.
175. Iribarren, A., E. Hernández-Rodríguez, and L. Maqueira, *Structural, chemical and optical evaluation of Cu-doped ZnO nanoparticles synthesized by an aqueous solution method.* Materials Research Bulletin, 2014. **60**: p. 376-381.
176. Kuriakose, S., B. Satpati, and S. Mohapatra, *Highly efficient photocatalytic degradation of organic dyes by Cu doped ZnO nanostructures.* Phys Chem Chem Phys, 2015. **17**(38): p. 25172-81.
177. Singh, B., et al., *Effect of Ni doping on structural and optical properties of Zn1− xNixO nanopowder synthesized via low cost sono-chemical method.* Materials Research Bulletin, 2015. **70**: p. 430-435.
178. Zamiri, R., et al., *Er doped ZnO nanoplates: Synthesis, optical and dielectric properties.* Ceramics International, 2014. **40**(1): p. 1635-1639.
179. Sajjad, M., et al., *Structural and optical properties of pure and copper doped zinc oxide nanoparticles.* Results in Physics, 2018. **9**: p. 1301-1309.
180. Usino, D.O., et al., *Influence of temperature and time on initial pyrolysis of cellulose and xylan.* Journal of Analytical and Applied Pyrolysis, 2020. **147**: p. 104782.
181. Ashok, A., et al., *Cellulose assisted combustion synthesis of porous Cu–Ni nanopowders.* RSC Advances, 2015. **5**(36): p. 28703-28712.
182. Vijay, R., et al., *Characterization of raw and alkali treated new natural cellulosic fibers from Tridax procumbens.* International journal of biological macromolecules, 2019. **125**: p. 99-108.
183. Rafique, S., et al., *Fabrication of silver-doped zinc oxide nanorods piezoelectric nanogenerator on cotton fabric to utilize and optimize the charging system.* Nanomaterials and Nanotechnology, 2020. **10**: p. 1847980419895741.
184. Johar, N., I. Ahmad, and A. Dufresne, *Extraction, preparation and characterization of cellulose fibres and nanocrystals from rice husk.* Industrial Crops and Products, 2012. **37**(1): p. 93-99.
185. Prithivirajan, R., et al., *Characterization of cellulosic fibers from Morus alba L. stem.* Journal of Natural Fibers, 2019. **16**(4): p. 503-511.

186. Muthukumaran, S. and R. Gopalakrishnan, *Structural, FTIR and photoluminescence studies of Cu doped ZnO nanopowders by co-precipitation method.* Optical Materials, 2012. **34**(11): p. 1946-1953.

187. Vijayaprasath, G., et al., *Comparative study of structural and magnetic properties of transition metal (Co, Ni) doped ZnO nanoparticles.* Journal of Materials Science: Materials in Electronics, 2015. **26**(9): p. 7205-7213.

188. Xiong, G., et al., *Photoluminesence and FTIR study of ZnO nanoparticles: the impurity and defect perspective.* physica status solidi c, 2006. **3**(10): p. 3577-3581.

189. Siddiquey, I.A., et al., *Sonochemical synthesis, photocatalytic activity and optical properties of silica coated ZnO nanoparticles.* Ultrasonics sonochemistry, 2012. **19**(4): p. 750-755.

190. Banu Bahşi, Z. and A.Y. Oral, *Effects of Mn and Cu doping on the microstructures and optical properties of sol–gel derived ZnO thin films.* Optical Materials, 2007. **29**(6): p. 672-678.

191. Hou, C., B. Hu, and J. Zhu, *Photocatalytic degradation of methylene blue over TiO2 pretreated with varying concentrations of NaOH.* Catalysts, 2018. **8**(12): p. 575.

192. He, J., et al., *Performance Promotion of Ag2O Photocatalyst by Particle Size and Crystal Surface Regulation.* New Journal of Chemistry, 2020.

193. Wang, Y., et al., *Facile synthesis of p-type Cu2O/n-type ZnO nano-heterojunctions with novel photoluminescence properties, enhanced field emission and photocatalytic activities.* Nanoscale, 2012. **4**(24): p. 7817-24.

194. Zelekew, O.A., et al., *Synthesis of efficient silica supported TiO2/Ag2O heterostructured catalyst with enhanced photocatalytic performance.* Applied Surface Science, 2017. **410**: p. 454-463.

195. Wang, Y., et al., *Ag2O/TiO2/V2O5 one-dimensional nanoheterostructures for superior solar light photocatalytic activity.* Nanoscale, 2014. **6**(12): p. 6790-6797.

196. Kadam, A., et al., *Template free synthesis of ZnO/Ag2O nanocomposites as a highly efficient visible active photocatalyst for detoxification of methyl orange.* J Photochem Photobiol B, 2016. **154**: p. 24-33.

197. Becerra, M.E., et al., *Decomposition of the Methylene Blue Dye Using Layered Manganese Oxide Materials Synthesized by Solid State Reactions.* International Journal of Chemical Engineering, 2018. **2018**: p. 4902376.

198. Huang, F., et al., *Analysis of the degradation mechanism of methylene blue by atmospheric pressure dielectric barrier discharge plasma.* Chemical Engineering Journal, 2010. **162**(1): p. 250-256.

199. Shidpour, R., et al., *Photo-degradation of organic dye by zinc oxide nanosystems with special defect structure: Effect of the morphology and annealing temperature.* Applied Catalysis A: General, 2014. **472**: p. 198-204.

200. Zhou, H., T. Fan, and D. Zhang, *Biotemplated materials for sustainable energy and environment: current status and challenges.* ChemSusChem, 2011. **4**(10): p. 1344-87.

201. Raj, R., *Fundamental research in structural ceramics for service near 2000 C.* Journal of the American Ceramic Society, 1993. **76**(9): p. 2147-2174.

202. Wang, D., et al., *Design and construction of the sandwich-like Z-scheme multicomponent CdS/Ag/Bi 2 MoO 6 heterostructure with enhanced photocatalytic performance in RhB photodegradation.* New Journal of Chemistry, 2016. **40**(10): p. 8614-8624.

Appendix

On this part, we have tried to generalize the data which were not mentioned on the main body of this thesis work. Hence we have tried to include the UV–vis absorption spectra of synthesized Z, A, CZ-1, CZ-3, CZ-4, CZA-6.8, CZA-13.6 and CZA-20.4 based catalysts.

Appendix I

UV-vis absorption spectra of Z, CZ-1, CZ-3, and CZ-4 catalysts

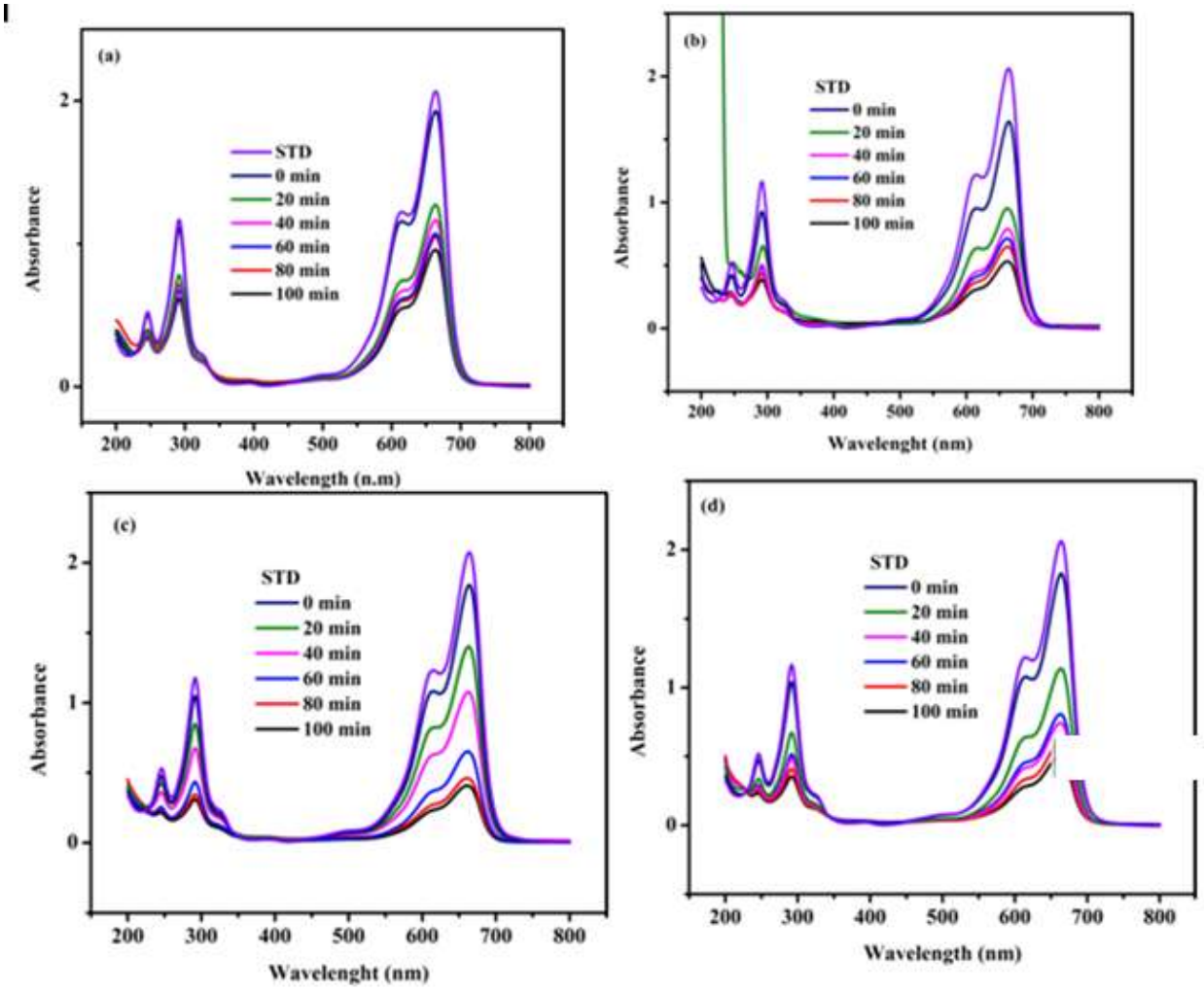

Figure 1. UV-vis spectra of Z (a), CZ-1 (b), CZ-3 (c) and CZ-4 (d) catalysts

Appendix II

UV-vis absorption spectra of A, CZA-6.8, CZA-13.6, and CZA-20.4 catalysts

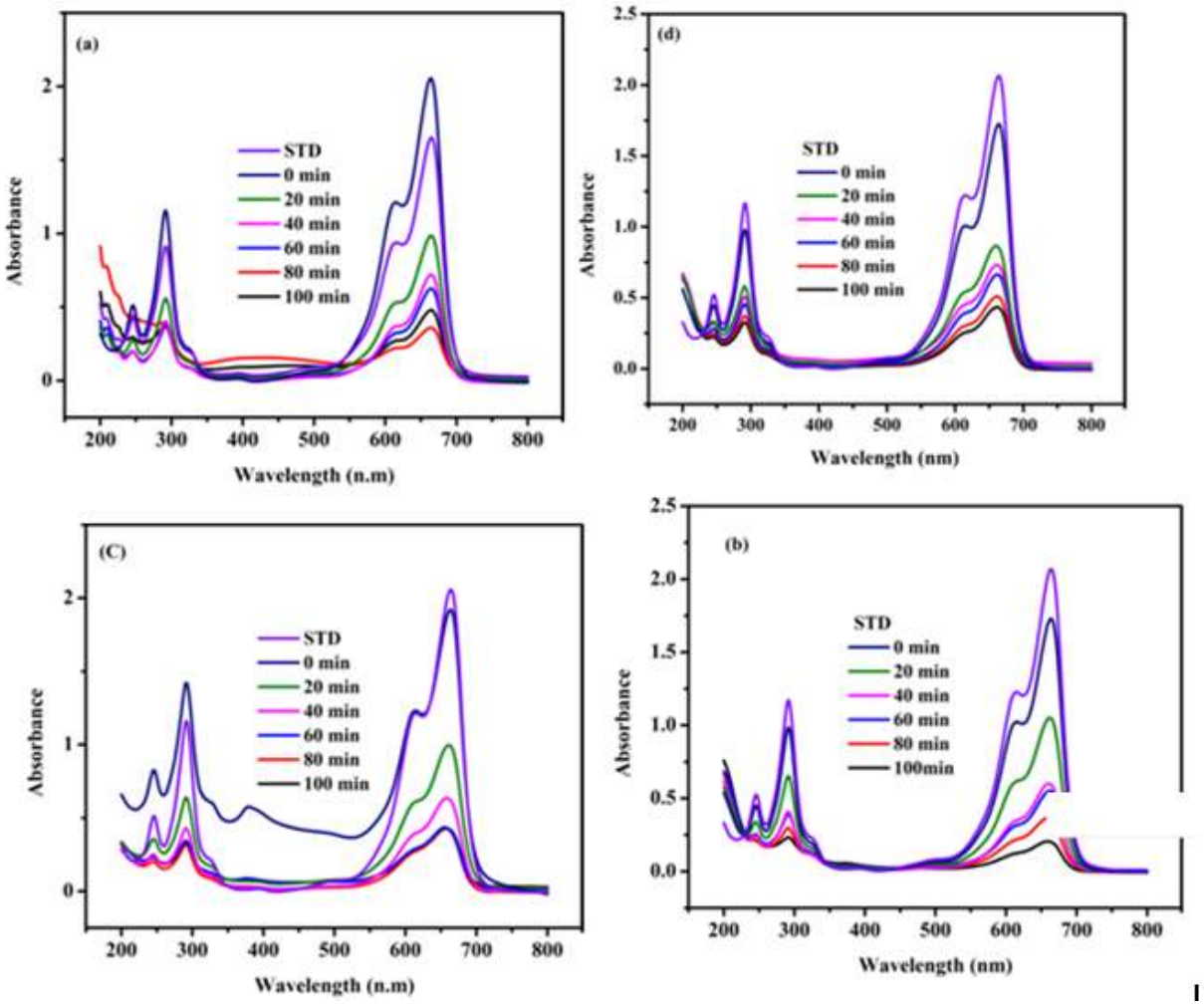

Figure 2. UV-vis spectra of A (a), CZA-6.8 (b), CZA-13.6 (c) and CZA-20.4 (d) catalysts

Appendix III

UV-vis absorption spectra of bare CZ-2 and bare CZA-10.2 (without Cellulose mediation)

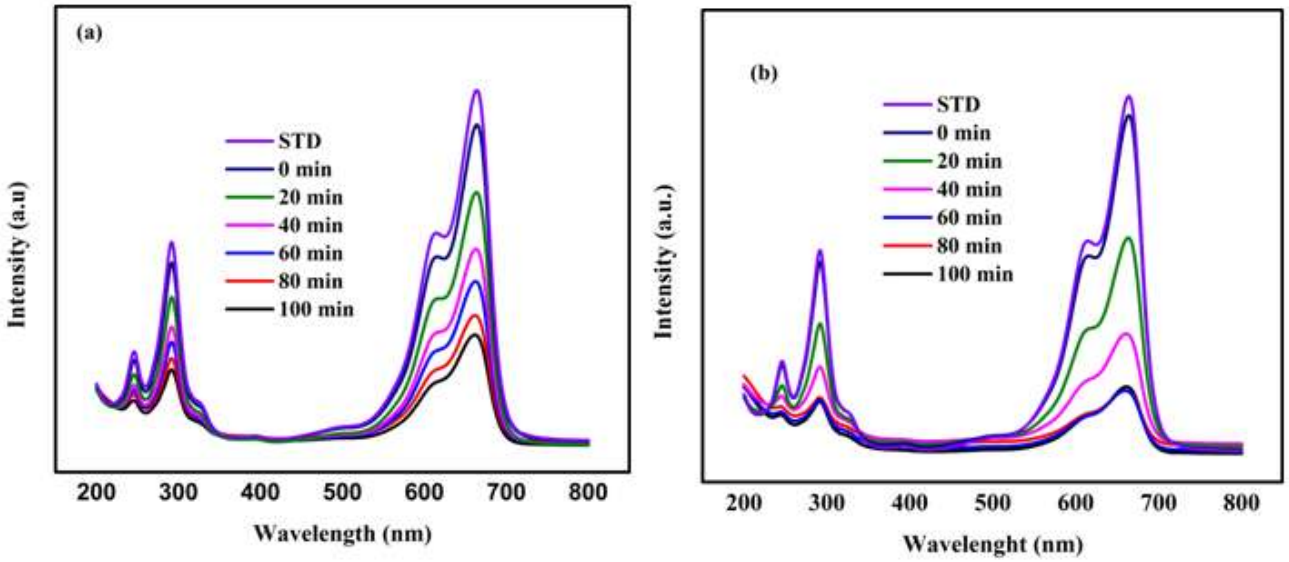

Figure 3. UV-vis spectra of bare CZ-2 (a) and bare CZA-10.2 (b)